Nanoscale

Accepted Manuscript

This article can be cited before page numbers have been issued, to do this please use: C. Adam, A. R. Piacenti, Y. Zhang, S. L. Waters and S. Contera, *Nanoscale*, 2025, DOI: 10.1039/D5NR01790D.

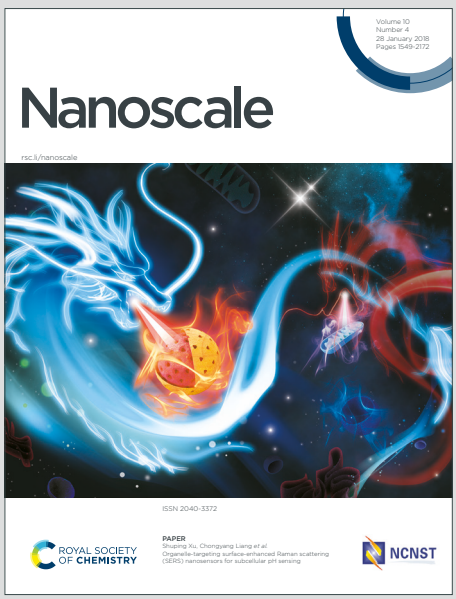

ROYAL SOCIETY OF CHEMISTRY

rsc.li/nanoscale

View Article Online
DOI: 10.1039/D5NR01790D

Viscoelastic Time Responses of Polymeric Cell Substrates Measured Continuously from 0.1-5,000 Hz in Liquid by Photothermal AFM Nanorheology

Casey Erin Adam,[†,‡] Alba Rosa Piacenti,[†] Yuanmin Zhang,[†] Sarah L. Waters,[‡] and Sonia Contera[*,†]

†*Department of Physics, University of Oxford, Parks Road, Oxford, OX1 3PU, UK*

‡*Department of Applied Mathematics, University of Oxford, Andrew Wiles Building, Radcliffe Observatory Quarter (550), Woodstock Road, Oxford, OX2 6GG, UK*

E-mail: sonia.antoranzcontera@physics.ox.ac.uk

Abstract

The mechanical properties of the polymeric substrate or matrix where a cell grows affect cell behavior. Most studies have focused on relating elastic properties of polymeric substrates, which are time-independent, to cell behaviors. However, polymeric substrates and biological systems exhibit a time-dependent, often viscoelastic, mechanical response. While less is known about how time responses dictate cell behavior, cells are likely sensitive to substrate time responses rather than elasticity alone. However, testing this hypothesis is complex due to the lack of nanoscale tools. To overcome this limitation, photothermal actuation-atomic force microscopy nanoscale dynamic mechanical analysis (PT-AFM nDMA), a novel AFM technique that measures sample viscoelasticity over a broad and continuous frequency range, was applied to measure the

View Article Online
DOI: 10.1039/D5NR01790D

viscoelastic properties of cell culture substrates made of poly(2-hydroxyethyl methacrylate) (poly(HEMA)) and collagen I (pureCol) in liquid at frequencies ranging continuously from 0.1 Hz - 5,000 Hz. PT-AFM nDMA to date has not been performed in liquid, but successfully and accurately characterized substrate viscoelasticity and synergized with measurements obtained using a more established AFM technique, bimodal imaging. The results of this study demonstrate that PT-AFM nDMA can be performed in liquid environments, especially relevant to biological samples. Additionally, comparing PT-AFM nDMA measurements of the poly(HEMA) and pureCol substrates in this study to cell behaviors described in the scientific literature on similar substrates suggests that longer substrate time responses at low measurement frequencies promote cell attachment, proliferation, and migration, while shorter substrate time responses promote ECM remodeling and differentiation.

Contents

View Article Online
DOI: 10.1039/D5NR01790D

1 Introduction

The mechanical properties of a cell's environment, especially those of the polymeric substrate on which the cell is located, play a crucial role in modulating cell activities.[1–6] Therefore, quantifying mechanical properties of substrates at length scales relevant to cells, the nanoscale and microscale, can provide insight into cell functions on the given substrate. Polymeric structures and biological systems exhibit characteristic time delays, called time responses, in response to an applied force or deformation.[7,8] In most cases, this time dependent response is viscoelastic.[7,8] Time responses (τ) dictate the propagation and attenuation of forces, and represent a combined metric of viscosity (η) and elasticity (E) of the system.[7,9] For commonly used models of viscoelasticity that apply to biological systems, $\tau = \eta/E$.[7,9] Biological systems typically contain multiple components, or even multiple configurations of a single component, and each component or configuration can possess a unique E, η, and τ. Therefore, biological systems typically exhibit multiple τ.

It is already established that E, η, and τ of a substrate influence cell behaviors. For example, substrate E alters proliferation and survival,[10–14] differentiation,[11,12,15–26] migration,[27–35] morphology,[12,36–39] cytoskeletal properties and adhesion,[23,40–46] plasma membrane

View Article Online
DOI: 10.1039/D5NR01790D

structure,[30,47,48] cell signaling and gene expression,[14,24,30,34,35,38,49–56] and other cell activities.[6,26,34,35,57–59] Substrate η, as well as that of the surrounding fluid (hydration shells or the bulk fluid), is as important as E in dictating cell behaviors.[60–73] Since τ dictates propagation and attenuation of forces,[7,9] it is reasonable to hypothesize that certain τ promote certain cell behaviors. Experiments that focus on the effect of substrate τ suggest that shorter τ promote ECM deposition and remodeling, as well as differentiation of cells within the substrate,[61] while longer τ seem to exhibit the opposite effects.[60] However, further investigation is required because the majority of studies quantify only substrate E or stiffness. Thus, the relation between substrate τ and cell behaviors is less understood than that of substrate E and cell behaviors.

Atomic force microscopy (AFM) is a particularly useful tool to measure nanoscale mechanical properties because AFM can probe a sample with angstrom resolution, can measure changes in forces as small as 10s of pN, can be performed in liquid, does not require sample processing such as fixation, can be performed on living samples, and has higher resolution and more localized control than other techniques such as optical and magnetic tweezers.[74,75] Several recent AFM advances have increased the ease of quantifying sample viscoelasticity, thereby enhancing the possibility of further studying the relationship between cell behavior and substrate mechanics. Such techniques include bimodal imaging, which measures nanoscale viscoelasticity at discrete frequencies, typically in the kHz range,[74,76–87] and has already been used to study a variety of biological samples.[82,83] The most common form of bimodal AFM is amplitude modulation-frequency modulation AFM (AM-FM AFM).[76,77,83] However, viscoelasticity is time dependent, meaning the frequency at which a sample is deformed determines the viscoelastic response, and it is therefore important to measure sample viscoelasticity over a range of frequencies.[7,9] Such nanoscale rheology can be performed with AFM techniques such as piezoelectric[88–105] or photothermal[106,107] actuation AFM nanoscale dynamic mechanical analysis (PE-AFM nDMA and PT-AFM nDMA, respectively), which measure sample viscoelasticity over a continuous frequency range that

View Article Online
DOI: 10.1039/D5NR01790D

spans several orders of magnitude.[106,107] PE-AFM nDMA is an established technique where either the cantilever holder or the sample are oscillated via PE actuation.[88–105] However, PE actuation introduces spurious resonance effects which are more pronounced in liquid and limit PE-AFM nDMA capabilities,[88,89,89–93,97,98,107–111] even when compensations for such resonances are performed.[88,89,89–93,97,98,111] Unlike PE-AFM nDMA, PT-AFM nDMA excites only the cantilever, thereby eliminating extra resonances due to sample or holder oscillation and increasing the range of frequencies at which sample mechanics can be measured.[107] However, PT-AFM nDMA is a novel technique that to date has only been performed on samples in air.[107] Therefore, investigation of whether PT-AFM nDMA can be performed in liquid without resonance and other liquid effects is required.

The purpose of experiments in this article is twofold. First, since PT-AFM nDMA is a novel technique[106,107] that has yet to be performed in liquid environments, this article provides a detailed analysis (supplementary material sections S7-S11) of how to perform PT-AFM nDMA in liquid to ensure that features such as damping due to fluid effects do not interfere with PT-AFM nDMA measurements, and to demonstrate that PT-AFM nDMA results are robust, even in liquid. Second, AM-FM AFM and PT-AFM nDMA were combined in order to quantify the nanoscale viscoelasticity, in particular τ, of widely used cell culture substrates in liquid, then correlate τ of each substrate with known cell behaviors on similar substrates. Six different substrates: three consisting of poly(2-hydroxyethyl methacrylate), poly(HEMA)[112,113] at different concentrations, and three collagen I substrates with varying amounts of crosslinking[114,115] were measured. These substrates were selected because cell behaviors on each substrate are well characterized in the literature,[13,22,27,114,114–126] both substrates are widely used in industry and research, and the macroscale mechanical properties of these substrates are well studied.[65–71,113,127–135] Both poly(HEMA)[127–131] and collagen I[65–71,132–135] substrates are viscoelastic.

View Article Online
DOI: 10.1039/D5NR01790D

2 Materials and methods

In order to study the relationship between substrate mechanics, in particular time responses, and cell behaviors, amplitude modulation-frequency modulation atomic force microscopy (AM-FM AFM, technique details in supplementary section S2) and photothermal actuation AFM nanoscale dynamic mechanical analysis (PT-AFM nDMA, technique details in supplementary section S5) were used to measure the viscoelastic properties of cell culture substrates at the nanoscale. Six substrates: three substrates synthesized with different concentrations of poly(HEMA), and three pureCol substrates with different amounts of crosslinking, were measured. One additional substrate, made of polydimethylsiloxane (PDMS), was measured in supplementary section S10 to assess the limits of PT-AFM nDMA in liquid.

Poly(HEMA) substrates strongly influence cell behaviors,[112] and are used in biomedical applications such as cell culture, contact lenses, fillings, histology, immobilization of cells and drugs, and implants.[113] The thickness of poly(HEMA) films modulates cell spreading and activities.[112,113] Higher concentrations of poly(HEMA) within a substrate hinder cell attachment, spreading, and DNA synthesis.[112,113] Substrates with high concentrations of poly(HEMA) have also been shown to decrease DNA synthesis in bovine aortic endothelial cells,[112] alter cytoskeleton (actin) dynamics in neutrophils,[136] alter leukocyte locomotion, force malignant melanoma cells to assume a round morphology and form polykaryons (multiple nuclei within a single cell), and decrease adrenal tumor cell synthesis of steroids.[113] Additionally, the viscoelastic properties of neutrophils are altered on poly(HEMA), compared to glass substrates.[136]

Collagen I is a widely used cell culture substrate[114,115] because collagen is the most prevalent protein in the human body, and collagen I is the most common form of collagen.[115–119] The mechanical properties of collagen I substrates regulate cell proliferation[13] and survival,[115] affect ECM deposition and remodeling,[120] regulate stem cell differentiation,[22] and regulate cell migration.[27] One commonly used collagen I substrate is known as pureCol^{TM}.[114] PureCol is a ready-made solution of purified collagen I isolated from bovine

View Article Online
DOI: 10.1039/D5NR01790D

skin and suspended in cell culture medium.[137] PureCol substrates affect cell morphology, proliferation, and viability.[114] Additionally, the elasticity of pureCol substrates is known to influence cell migration.[121] An additional benefit from the use of pureCol and similar collagen I substrates is that the mechanical properties of the substrates are tuneable via the use of crosslinking agents such as glutaraldehyde (GA).[122–126] Therefore, collagen substrates are convenient for studying how varying the mechanical properties of a substrate alter cell behaviors and mechanics.

All poly(HEMA) and pureCol substrates were measured in live cell imaging solution (Sigma-Aldrich A14291DJ), which mimics physiological salt concentrations. Live cell imaging solution consists of 140 mM NaCl, 2.5 mM KCl, 1.8 mM $CaCl_2$, 1.0 mM $MgCl_2$, and 20 mM (4-(2-hydroxyethyl)-1-piperazineethanesulfonic acid) (HEPES) at pH 7.4 and with an osmolarity of 300 mOsm.[138] The PDMS substrate was measured in milliQ water, as detailed in supplementary section S10. Table 1 summarizes the expected outcomes of PT-AFM nDMA measurements for pureCol and poly(HEMA) substrates. Additional details describing how these expected results were obtained can be found in supplementary section S12.

2.1 Poly(HEMA) Substrate Synthesis

Synthesis of poly(HEMA) substrates was carried out per the standard protocol.[112] Briefly, 6 g of poly(HEMA) powder (Sigma-Aldrich P3932) were dissolved in 50 mL of 95% ethanol to create a stock poly(HEMA) solution of 120 mg poly(HEMA) per mL ethanol. This solution was left stirring overnight to ensure that the poly(HEMA) was fully solubilized. The next morning, to remove any undissolved poly(HEMA), the stock solution was centrifuged for 30 minutes at 2,500 rpm, then the supernatant was transferred to a new container. The resulting stock solution was then diluted serially in 95% ethanol, resulting in three different poly(HEMA) working solutions with: 120 mg poly(HEMA) per mL ethanol, 12 mg poly(HEMA) per mL ethanol, or 1.2 mg poly(HEMA) per mL ethanol. To prepare poly(HEMA) substrates, glass coverslips were sterilized with ethanol, placed in a petri dish,

View Article Online
DOI: 10.1039/D5NR01790D

Table 1: Expected PT-AFM nDMA measurement outcomes for poly(HEMA) substrates and pureCol substrates crosslinked with glutaraldehyde (GA) for 30 minutes, 2 hours, or 24 hours. All expected results were obtained from macroscale rheology measurements over a range of measurement frequencies (f). Additional details describing how these expected results were obtained can be found in supplementary section S12.

Substrate	$\tan\delta$	E'	E''
poly(HEMA) Substrates[127,128]	Should be on the order of 10^{-1} at lower f, but increase to 10^{0} near $f = 100$ Hz	Should be on the order of 10^{3} - 10^{5} Pa and have no abrupt changes in slope for $f < 100$ Hz.	Should be on the order of 10^{3} - 10^{5} Pa and have no abrupt changes in slope for $f < 100$ Hz.
pureCol Substrates [67,122,132–135,139–142]	Should be on the order of 10^{-2} - 10^{-1} and have no abrupt changes in slope for $f < 600$ Hz	Should be on the order of 10^{2} - 10^{3} Pa, but could be as high as 10^{8} Pa, and have no abrupt changes in slope for $f < 600$ Hz	Should be on the order of 10^{1} - 10^{2} Pa, but could be as high as 10^{7} Pa, and have no abrupt changes in slope for $f < 600$ Hz
GA effects on pureCol[122,140–142]	Should be 1.2 - 4x higher for 30 min GA crosslinking than 2 hr or 24 hr, and should be similar for the 2 hr and 24 hr GA samples.	The 2 hr and 24 hr GA samples should be more similar to each other than the 30 min GA sample. E' will either increase or decrease with increased GA crosslinking, but direction is unclear due to conflicting literature reports.	Should follow similar trends to E'

and left to dry. The desired solution of poly(HEMA) was then pipetted onto the coverslip, at 95.2 μL poly(HEMA) solution per cm^2 of coverslip surface area,[112] resulting in substrates with 11.4 mg poly(HEMA) per cm^2 of coverslip surface area, 1.14 mg poly(HEMA) per cm^2, and 0.114 mg poly(HEMA) per cm^2. This standard protocol results in poly(HEMA) films roughly 35 μm, 3.5 μm, and 0.35 μm thick, respectively, for the 11.4, 1.4, and 0.114 mg poly(HEMA) per cm^2 substrates.[112]

Once poly(HEMA) solutions were deposited onto coverslips, the sample was left to dry at room temperature for 48 hours to ensure that all the ethanol had evaporated. After drying for 48 hours, coverslips with dry poly(HEMA) substrates were secured to a magnetic disk, which holds the sample in place during AFM measurements, using double-sided foam (RS Components 554-844), and transferred to an Oxford Instruments Asylum Research Cypher ES AFM. In order to simulate physiological conditions, 200 - 400 μL of live cell imaging

View Article Online
DOI: 10.1039/D5NR01790D

solution (Sigma-Aldrich A14291DJ) were then pipetted onto the sample. Measurements were obtained at least 30 minutes after live cell imaging solution was added in order to allow the poly(HEMA) substrates to fully swell.[112]

2.2 PureCol Substrate Synthesis

Synthesis of pureCol substrates was carried out per the protocol specified by the manufacturer.[137] Briefly, pureCol^{TM} EZ Gel solution (Sigma-Aldrich 5074) was stored at 4^{o}C, to prevent gelation. To form pureCol substrates, 200 μL of pureCol were added to a custom sample chamber 0.8 cm x 0.6 cm x 0.3 cm (length, width, height) made of double-sided foam (RS Components 554-844). Sample chambers were created by cutting 0.8 cm x 0.6 cm rectangles out of double-sided foam with a scalpel, stacking three such strips on top of one uncut strip, and securing the resulting chamber to a magnetic disk, which holds the sample in place during AFM measurements. Supplementary figure S11A shows this custom chamber. Supplementary figure S11B shows the chamber once 200 μL pureCol have been added. Custom chambers were used because the pureCol substrates often detached from coverslips, and therefore were not immobilized enough to measure with the AFM, and petri dishes were too large to fit inside the Cypher AFM.

After pureCol was added to the custom chamber, the chamber was incubated at 37^{o}C for 90 minutes to allow the collagen to polymerize. The resulting substrate is shown in Supplementary figure S11C. While the collagen polymerized, a 50% glutaraldehyde (GA) solution in water (Sigma-Aldrich 340855) was diluted in Dulbecco's phosphate buffered saline (DPBS, Sigma-Aldrich D5796) to a final concentration of 1% GA in DPBS. Once polymerization was complete, 400 μL of the 1% GA in DPBS were deposited on top of the pureCol (supplementary figure S11D). Samples were then left to crosslink in GA at room temperature for: 30 minutes, 2 hours, or 24 hours. GA crosslinking durations were based on those used in the literature to alter the number of crosslinks between the three substrates.[123–125] This particular crosslinking procedure was adopted for reasons detailed in results section 3.1. After

View Article Online
DOI: 10.1039/D5NR01790D

GA crosslinking was complete, samples were washed three times via the following procedure. First, any liquid was pipetted off the sample. Next, 400 μL of DPBS were pipetted onto the samples and left to sit for five minutes. This procedure was repeated three times. After the final wash, the DPBS was removed, and replaced with 400 μL of live cell imaging solution (Sigma-Aldrich A14291DJ). A completed sample is shown in supplementary figure S11E, and was roughly 0.3 cm thick. The sample was then transferred to an Oxford Instruments Asylum Research Cypher ES AFM.

2.3 Principles of AM-FM AFM and PT-AFM nDMA

Both AM-FM AFM and PT-AFM nDMA are dynamic experiments,[76,83,107,143] meaning that an oscillation is applied to a sample and dynamic sample properties are measured.[7,144] These dynamic properties are the storage modulus (E', measured by both techniques), loss modulus (E'', measured only by PT-AFM nDMA), and loss tangent ($\tan\delta = E''/E'$, measured by both techniques).[76,83,107,143] All three properties are functions of sample E and η, and by extension τ, since $\tau = \eta/E$.[7,144] The exact formula relating E and η to E', E'', and $\tan\delta$ depends on the type of viscoelasticity exhibited by a sample (details and formulas are provided in supplementary section S1),[7,144] and can be determined from dynamic measurements.[87,144]

AM-FM AFM measures sample $\tan\delta$ and E' at one specific frequency, and $\tan\delta$ corresponds to a different frequency than E'.[76,77,83] In AM-FM AFM, the surface of a sample is intermittently tapped via a tip connected to a cantilever that is oscillated at two of the cantilever's eigenmodes.[76,77,83] Cantilever properties at each mode include: frequency f_c, stiffness k_c, and the resonance peak at f_c has quality factor Q_c.[76,77,83] The cantilever's vibration at each eigenmode has amplitude A_r far from the sample, amplitude A on the sample, and phase ϕ.[76,77,83] These properties of the cantilever (k_c, Q_c, f_c) and bimodal oscillation (A_r, A, ϕ) at each eigenmode (subscript 1 for the lower frequency mode, 2 for the higher frequency mode) are used to calculate sample $\tan\delta$ at f_1 via equation 1[84,85] and E' at f_2 via equation 2.[76,86] Additional details on how these formulas are derived and the operating

View Article Online
DOI: 10.1039/D5NR01790D

principles of AM-FM AFM can be found in supplementary section S2.

$$\tan\delta = \frac{\sin(\phi_1) - \frac{A_1}{A_{r,1}}}{\cos(\phi_1)} \tag{1}$$

$$E'_{t/s} = \frac{4\sqrt{2A_1}k_{c,2}^2 Q_{c,1}\left(\Delta f_{c,2}\right)^2}{\sqrt{R}k_{c,1}A_{r,1}f_{c,2}^2\cos\phi_1} \tag{2}$$

Here, $E'_{t/s}$ is the contact modulus which converts to sample E'.[76,86] Note that, to obtain equation 2, the Hertz contact model is used to describe the tip/sample interaction.[76,86] The Hertz model assumes an elastic, nonadhesive interaction between a spherical indenter and sample.[9,145] Therefore, AM-FM AFM quantification of E' can be incorrect if the tip/sample contact is non-Hertzian.[76,77,87,107]

The measured E' and $\tan\delta$ from all pixels of a single AM-FM AFM image can be used to determine the viscoelastic model which best describes sample behavior.[87,146] One model of viscoelasticity that is widely applicable to biological systems is the General Maxwell Model (GMM), also called the Wiechert model (supplementary equations S4, S14-S16).[7] Details of the GMM, as well as special cases of the GMM called the standard linear solid (SLS, supplementary equations S1, S11-S13), Kelvin-Voigt model (KV, supplementary equations S2, S8-S10), and Maxwell model (MW, supplementary equations S3, S5-S7) are provided in supplementary section S1. It is possible to use AM-FM AFM measurements to determine whether the GMM or special cases of the GMM describe a sample by plotting $y = \tan\delta^{-1}$ against $x = (E'\tan\delta)^{-1}$ and fitting a line with slope m and y-intercept b to the data.[87] If the fit has a low root mean square error (RMSE), then the GMM, SLS, KV, or MW model describes sample behavior.[87] If both $m > 0$ and $b > 0$, then the GMM or SLS describes the sample.[87] The GMM applies if the points from the fit appear curved, even though still well described by a line, while the SLS applies if the points appear linear.[87] If $m > 0$ and $b = 0$, then the KV model applies.[87] If $m = 0$ and $b > 0$, then the MW model applies.[87] This test can accurately determine the viscoelastic model to describe a sample even if the measured

View Article Online
DOI: 10.1039/D5NR01790D

E' is incorrect due to applying the Hertz model to a non-Hertzian tip/sample contact.[87]

While AM-FM AFM measures sample $\tan\delta$ and E' at different, discrete frequencies,[76,84–86] PT-AFM nDMA measures sample E', E'', and $\tan\delta$ over a continuous range of frequencies.[107] In PT-AFM nDMA, the sample is indented and allowed to fully relax, then the cantilever is oscillated via a chirped frequency signal, then withdrawn.[107] The same chirp measurement is repeated out of contact with the sample and acts as a reference measurement.[107] Cantilever A and ϕ at each measurement frequency are then compared between the sample (s) and reference (r) measurements to obtain $\tan\delta$ and the storage and loss stiffness (k' and k'', respectively) of the sample via equations 3-5.[90,104,107]

$$k' = k_c \left[\frac{A_r}{A_s} \cos\left(\phi_r - \phi_s\right) - 1 \right] \tag{3}$$

$$k'' = k_c \frac{A_r}{A_s} \sin\left(\phi_r - \phi_s\right) \tag{4}$$

$$\tan\delta = \frac{k''}{k'} \tag{5}$$

Finally, k' and k'' are converted to E' and E'' by applying a contact model.[107] Additional details of PT-AFM nDMA operating principles can be found in supplementary section S5.

AM-FM AFM uses the Hertz model to calculate sample E'.[76,86] Therefore, to keep the contact model consistent between measurement techniques in this article, the Hertz model was also applied to obtain PT-AFM nDMA E' and E'' (see supplementary equations S34 and S35). Other contact models, while likely more applicable, are not investigated in this study. The use of the Hertz model for AM-FM AFM[76,86] necessitates use of the Hertz model for PT-AFM nDMA to ensure that results from each technique can be compared. While doing so will affect E' and E'', the same is not true for $\tan\delta$.[87,107] Regardless of measurement technique, contact geometry cancels in $\tan\delta$, rendering $\tan\delta$ independent of contact mechanics.[87,107]

View Article Online
DOI: 10.1039/D5NR01790D

2.4 Measurement Procedure

For each substrate, AM-FM AFM was performed on the sample first. Second, PT-AFM nDMA was performed at specific points in the final AM-FM AFM image. All substrates were measured with AC240TSA cantilevers (Olympus, $k_1 \sim 1.6$ nN/nm, $k_2 \sim 58.8$ nN/nm, $f_1 \sim 21$ kHz in liquid, $f_2 \sim 150$ kHz in liquid, $R = 7 \pm 3$ nm) driven via photothermal actuation at full excitation laser (blueDrive$^{\text{TM}}$, Oxford Instruments Asylum Research, 405 nm wavelength) power. PureCol substrates were also measured with the short thin tip of an RC800PSA cantilever (Olympus, $k_{c,1} \sim 0.2$ N/m, $k_{c,2} \sim 18$ N/m, $f_{c,1} \sim 25$ kHz in liquid, $f_{c,2} \sim 170$ kHz in liquid, $R = 15 \pm 5$ nm) driven by photothermal excitation at 0.3x the maximum blueDrive$^{\text{TM}}$ power. Cantilevers were calibrated via the Oxford Instruments Asylum Research GetReal$^{\text{TM}}$ calibration method[143,147,148] to avoid blunting the tip. All experiments were performed using Oxford Instruments Asylum Research software version 16.9.220 in Igor Pro software version 6.38B01.

PureCol substrates were measured by two different cantilevers in order to assess how cantilever selection affected PT-AFM nDMA measurements. First, each cantilever was loaded into a separate holder, and the spring constant of both cantilevers was calibrated in air via the Oxford Instruments Asylum Research GetReal$^{\text{TM}}$ calibration method.[143,147,148] Next, the hydrated sample then the holder containing the RC800PSA were loaded into the Cypher, the RC800PSA's inverse optical lever sensitivity (InvOLS) was calibrated far from the sample, then AM-FM AFM and PT-AFM nDMA were performed using the RC800PSA. The cantilever holder containing the RC800PSA was then swapped for that containing the AC240TSA, AC240TSA InvOLS was calibrated far from the sample, then measurements were repeated with the AC240TSA. Thereby, the effect of cantilever selection was analyzed on measurements of the same substrate as close to the same location on the sample as possible. Poly(HEMA) substrates were only measured with AC240TSA cantilevers because RC800PSA cantilevers were too soft to accurately quantify poly(HEMA) sample properties.

View Article Online
DOI: 10.1039/D5NR01790D

2.4.1 PT-AFM nDMA Parameters

PT-AFM nDMA measurements excited each sample over a frequency range of 0.1 - 5,000 Hz. This frequency range was split into two or three different measurement regimes, in order to optimize the data sampling rate and avoid crashing the AFM software. For poly(HEMA) measurements, frequencies ranged from 0.1 - 10 Hz during a PT-AFM nDMA dwell of three minutes, from 0.5 - 100 Hz during a PT-AFM nDMA dwell of 60 seconds, and from 1 - 10,000 Hz during a PT-AFM nDMA dwell of 40 seconds. For pureCol, frequencies ranged from 0.1 - 10 Hz during a PT-AFM nDMA dwell of three minutes, and from 1 - 5,000 Hz during a PT-AFM nDMA dwell of 40 seconds. PT-AFM nDMA is an off resonance technique (see supplementary section S5.1).[107] Therefore, PT-AFM nDMA was not performed at frequencies higher than 5,000 Hz for RC800PSA measurements and 10,000 Hz for AC240TSA measurements in order to avoid introducing error caused by cantilever resonance effects. The drive amplitude of each chirp was 0.25 V, resulting in a maximum chirp amplitude of roughly 40 nm (at lower measurement frequencies) and a minimum chirp amplitude of roughly 2.5 nm (at higher measurement frequencies). Example plots of amplitude as a function of measurement frequency are shown in supplementary figure S9A and previously published.[106,107] Samples were indented to a force trigger point (see supplementary sections S4 and S8 for an explanation of indentation and trigger points) that resulted in a sample indentation between 100 nm and 600 nm, around which the PT-AFM nDMA measurement oscillated. Indentation depth was tailored for each sample as described in supplementary section S8 to ensure measurements were performed in the linear viscoelastic regime of the sample, where measurement values are independent of sample indentation.[9,107] Example indentations without the PT-AFM nDMA oscillation are shown in figure 1A,C and supplementary figure S10. Indentation approach and withdraw velocity was 1 μm s^{-1}, with an approach time of 5-15 s to allow full sample relaxation before performing the PT-AFM nDMA chirp.

View Article Online
DOI: 10.1039/D5NR01790D

2.4.2 Data Processing and Analysis

After each experiment, topography images from AM-FM AFM data were flattened using Oxford Instruments Asylum Research software version 16.9.220 in Igor Pro software version 6.38B01, in order to remove any variations in sample topography that were not due to substrate features. This flattening was done by hand, in order to avoid introducing flattening artifacts. The processed files were then analyzed by a custom script written in MATLAB R2019b. This custom script calculated $\tan\delta$ and E' of the substrates by applying equations 1 and 2 to AM-FM AFM data, then used these values to determine if the GMM or special cases of the GMM (model details can be found in supplementary section S1) applied to the substrate.[87,146] The custom script also calculated the mean and standard deviation of substrate feature height, E', and $\tan\delta$ by fitting a Gaussian to the distribution of values within a particular image or within the sample as a whole, as detailed in supplementary section S3. This method of calculating the mean and standard deviation was used in order to minimize the effects of bimodal or multimodal distributions of the data, shown in section 3.2.1. Comparison p-values were calculated from pairwise t-tests between the relevant samples.

Another custom script written in MATLAB R2019b 9.7.0.1261785 was used to analyze PT-AFM nDMA data. This script loaded sample and reference measurements, then applied equation 3 - 5 in order to calculate k' and k'', as well as $\tan\delta$ of the sample. Next, the Hertz contact model[9,76,86] was applied to calculate E' and E'' from k' and k'' via supplementary equations S34 and S35. The contact point, where the tip first touches the sample, was manually identified for application of the Hertz contact model. While other contact models likely better describe the tip/sample interaction during PT-AFM nDMA measurements, the Hertz model was applied to PT-AFM nDMA measurements in order to keep the contact model consistent between AM-FM AFM, which solely uses the Hertz model,[76,77,86] and PT-AFM nDMA. In order to reduce measurement artifacts arising from factors such as friction, which affected some of the lower frequency measurements, or Gibbs phenomena, which affected the higher frequencies of each chirp regime, the ends of each PT-AFM nDMA measurement were

View Article Online
DOI: 10.1039/D5NR01790D

trimmed, then measurements were smoothed using the Savitzky-Golay filter, as detailed in supplementary section S6, and shown in supplementary figure S3.

3 Results

It was necessary to optimize the synthesis of pureCol substrates because substrate properties varied depending on crosslinking procedure, affecting how the AFM probe interacted with the sample (section 3.1). Once samples stable enough to measure with the AFM tip were synthesized, AM-FM AFM (section 3.2) and PT-AFM nDMA (section 3.3) were performed at multiple points on poly(HEMA) and pureCol substrates to measure the effect of poly(HEMA) concentration and pureCol crosslinking on E', E'', and $\tan\delta$ of the substrates over a range of frequencies. Measurements were then averaged for each substrate, used to calculate substrate time responses, and compared across substrates (section 3.4).

3.1 Optimizing Synthesis of PureCol Substrates

Attempts at AFM measurements of pureCol substrates that were not crosslinked were performed using AC240TSA cantilevers (Olympus, $k_1 \sim 1.6$ nN/nm, $k_2 \sim 58.8$ nN/nm, $f_1 \sim 21$ kHz in liquid, $f_2 \sim 150$ kHz in liquid, $R = 7 \pm 3$ nm), RC800PSA cantilevers (Olympus, all four tips, but in particular the short thin tip with $k_{c,1} \sim 0.2$ N/m, $k_{c,2} \sim 18$ N/m, $f_{c,1} \sim 25$ kHz in liquid, $f_{c,2} \sim 170$ kHz in liquid, $R = 15 \pm 5$ nm), and Olympus bioLeverMini cantilevers. Regardless of the cantilever used, pureCol substrates that had not been crosslinked were too fluid to detect with the AFM tip. The tip would enter the pureCol substrate (visible on the optical microscope in the AFM), and the deflection would fluctuate, but the trigger point and/or setpoint was never reached. It was therefore necessary to crosslink pureCol substrates. Glutaraldehyde (GA) was used to crosslink the substrates.[123–125] Crosslink density within a pureCol substrate can be altered by changing the duration to which the substrate is exposed to GA, or by changing the GA concentration.[124,126]

View Article Online
DOI: 10.1039/D5NR01790D

Initial attempts to crosslink pureCol substrates were performed by varying the concentration of GA in the crosslinking solution to which the substrate was subjected for 30 min. GA concentrations of 0.01%, 1%, 2%, and 4% were used, based on previous literature.[124,126] Substrates crosslinked with 0.01% GA behaved in a similar manner to pureCol that was not crosslinked, and therefore could not be measured. Substrates crosslinked with 2% or 4% GA possessed a layer of loose surface material thicker than one μm (shown in figure 1B and D). It was not possible to perform AM-FM AFM on these substrates because the thick surface layer prevented a repulsive tip/sample interaction, which is required for AM-FM AFM measurements.[85] While it was possible to indent through the surface layer to the bulk pureCol substrate (indentation experiments are described in supplementary section S4), the thick surface layer caused spurious cantilever deflection during PT-AFM nDMA measurements, preventing accurate PT-AFM nDMA quantification of sample properties. These layers and layer effects were reproducible, and occurred in two to three samples for each (2% and 4%) GA concentration. Substrates crosslinked with 1% GA did not exhibit thick surface layers (figure 1A and C). Therefore, subsequent attempts to crosslink pureCol substrates were performed by varying the time to which the substrate was exposed to 1% GA, with longer exposure times resulting in more crosslinks.[123–125] PureCol samples exposed to GA for 4 hours also exhibited thick surface layers. However, samples crosslinked for 30 minutes, 2 hours, and 24 hours did not have surface layers (figure 1C), or surface layer thickness was small enough not to impede measurements (figure 1A).

The surface layer on pureCol substrates is most likely a polymer brush.[149] Such brushes can form as the result of loose polymer ends protruding from the surface of the substrate, and can range from tens or hundreds of nanometers[150,151] to several microns in thickness.[149,152] Additionally, loose ends of collagen fibrils in tendons can behave as polymer brushes.[153] These results demonstrate that, if a sample contains thick polymer brushes or other surface effects, the reference measurement for PT-AFM nDMA may be unable to account for such effects, and PT-AFM nDMA will therefore be unable to accurately measure sample properties.

View Article Online
DOI: 10.1039/D5NR01790D

Additionally, these effects may be more pronounced in liquid, where substrates swell and loose polymer ends floating at the substrate surface are freer to move[7] and interact with the tip and cantilever. Such surface effects are investigated in greater detail in supplementary

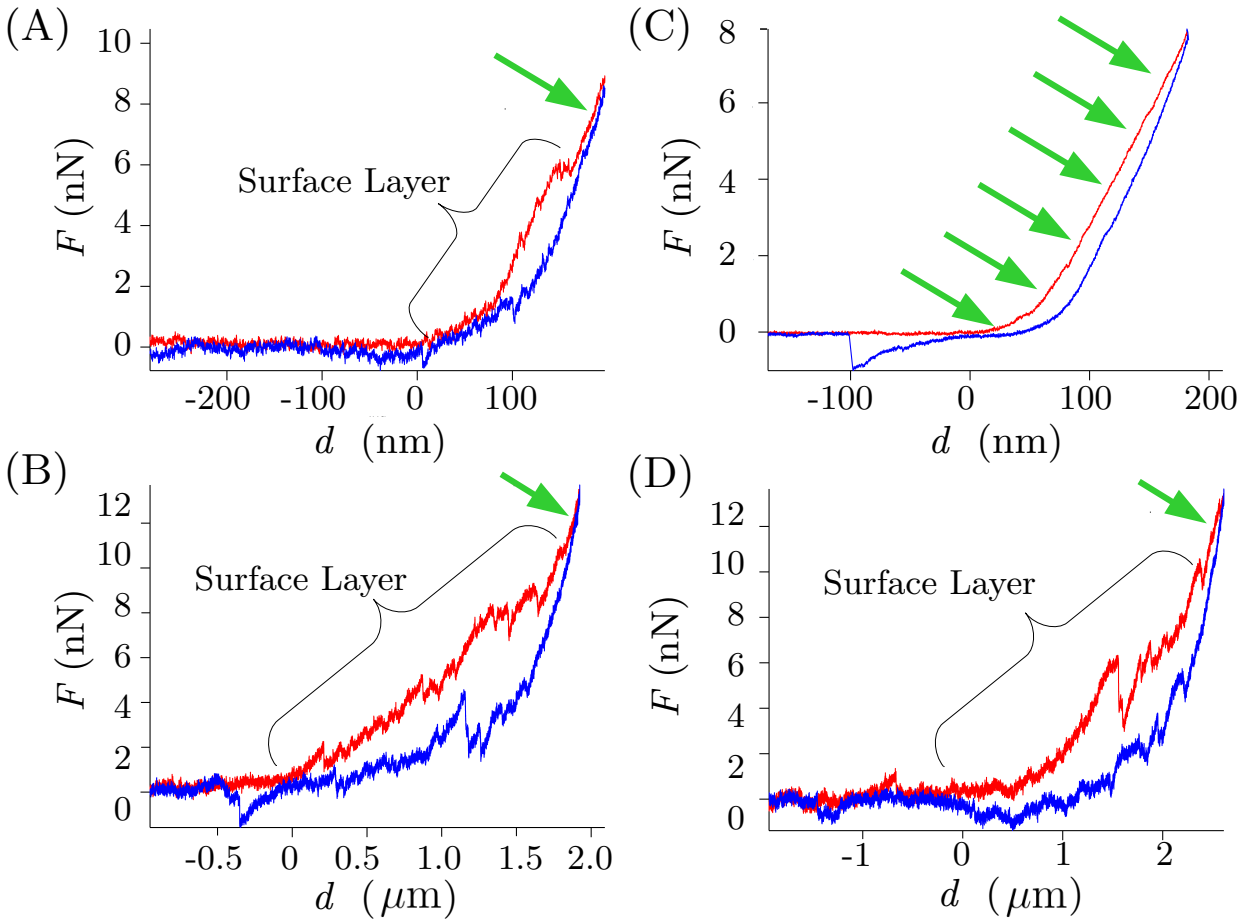

Figure 1: Example pureCol substrate indentation curves. During indentations, an AFM tip is pressed into a sample (red curve) then retracted (blue curve).[74] The force, F, experienced by the cantilever and sample indentation, d, are tracked throughout.[74] More details on indentations can be found in supplementary section S4. A typical F vs. d curve obtained with an AC240TSA cantilever on pureCol substrates that could be measured with AM-FM AFM and PT-AFM nDMA is shown in (A). Green arrows indicate the force curve region where the bulk pureCol is indented. Bumps in the approach curve (black brackets), indicate that the tip passed through a surface layer of material roughly 150 nm thick, likely a polymer brush, before reaching the bulk. (B) shows an AC240TSA F vs. d curve of a pureCol substrate with a surface layer thicker than 1 μm, which prevented AM-FM AFM or PT-AFM nDMA from accurately quantifying sample viscoelasticity. (C) shows a representative F vs. d curve obtained with an RC800PSA cantilever on the same substrate as (A), indicating that the RC800PSA was less sensitive to the substrate's surface layer than the AC240TSA. (D) shows an RC800PSA F vs. d curve of a substrate with a thick surface layer, similar to (B).

View Article Online
DOI: 10.1039/D5NR01790D

section S10.

AC240TSA cantilevers (figure 1A) were more sensitive to the pureCol surface layer than RC800PSA cantilevers on the same substrate (figure 1C). The higher stiffness of AC240TSA cantilevers means that less energy from tip/sample interactions would be dissipated by the cantilever, thereby rendering AC240TSA cantilevers more sensitive to vibrations caused by interactions with the substrate's surface layer. Therefore, in agreement with previous literature,[107] cantilever selection will likely affect PT-AFM nDMA measurements. Additional analysis of cantilever selection on PT-AFM nDMA measurements in liquid is provided in supplementary section S9.

3.2 AM-FM AFM Measurements of Cell Culture Substrates

AM-FM AFM was performed to analyze nanoscale variation in sample E' and $\tan\delta$ (section 3.2.1), quantify sample properties at AM-FM AFM measurement frequencies (section 3.2.2), and determine the type of viscoelasticity exhibited by each substrate (section 3.2.3). Details on the cantilever, scan dimensions, and number of pixels analyzed for each AM-FM AFM image in this article are provided in supplementary table S1. Sample indentations in AM-FM AFM are only a few nm deep,[77] constituting roughly 0.0001% of pureCol sample thickness and roughly 0.01%, 0.1%, and 1% of the 11.4, 1.14, and 0.114 mg poly(HEMA) per cm^2 substrate thickness, respectively.

3.2.1 Nanoscale Variation in Sample Properties

As shown in figure 2, individual AM-FM AFM images exhibited varying distributions of E' and $\tan\delta$, indicating local variation in sample mechanics at the nanoscale. Typically, these distributions were best described with a two term Gaussian model (details in supplementary section S3, supplementary equation S27). Since only a single substrate was imaged at a given time, different peaks in the two term Gaussian fits correspond to various structures or orientations of the substrate's constituent polymers.

View Article Online
DOI: 10.1039/D5NR01790D

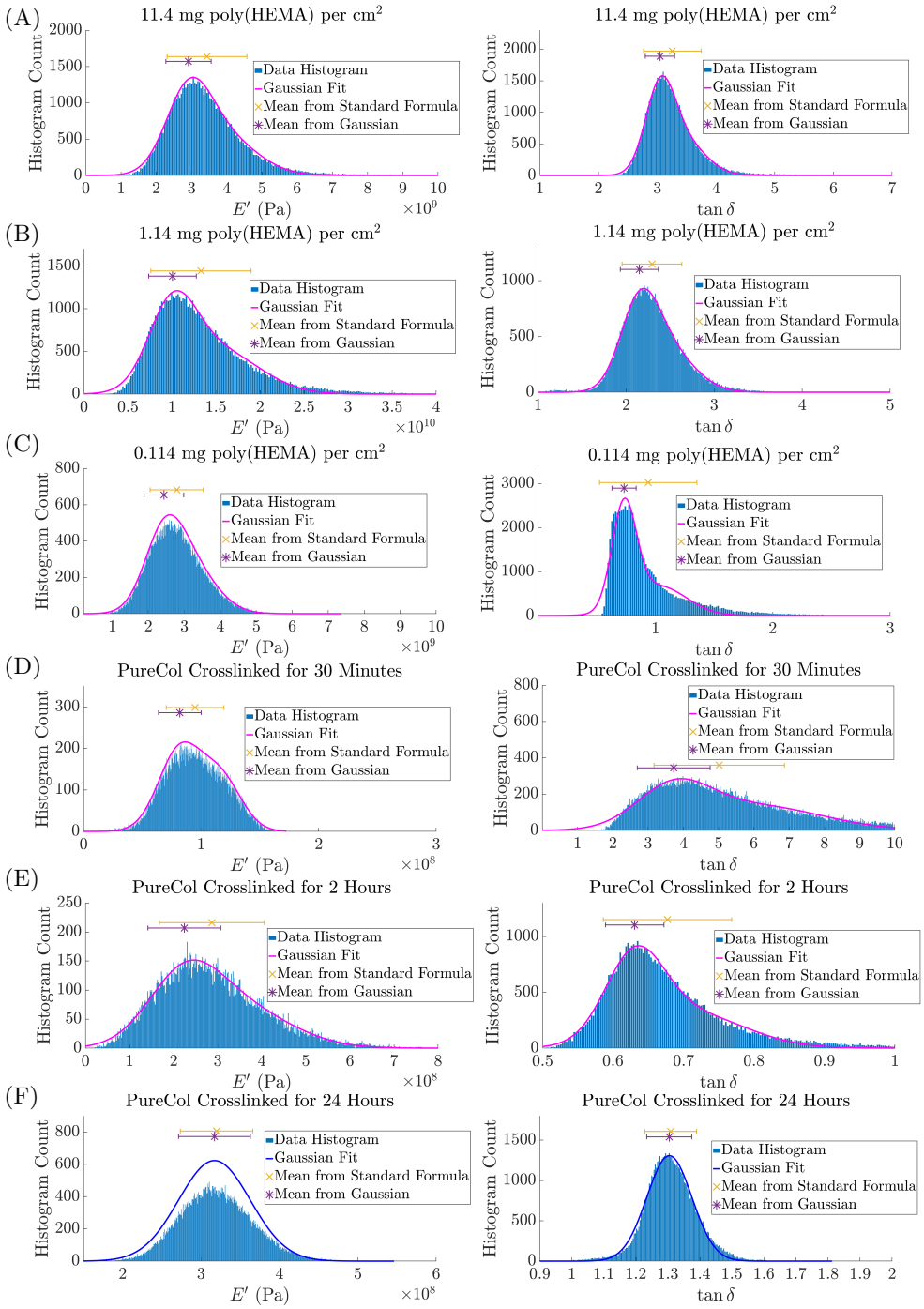

Figure 2: Representative distributions from AM-FM AFM measurements of cell culture substrates. All distributions were obtained from a single AM-FM AFM image. Storage modulus, E', and loss tangent, $\tan\delta$, distributions are shown in the left and right column, respectively, for substrates of: 11.2 mg poly(HEMA) per cm^2 of sample surface area (A), 1.12 mg poly(HEMA) per cm^2 (B), 0.112 mg poly(HEMA) per cm^2 (C), pureCol crosslinked with glutaraldehyde for 30 minutes (D), pureCol crosslinked for 2 hours (E), and pureCol crosslinked for 24 hours (F). A Gaussian fit to the distribution, described in supplementary section S3, is shown as a magenta line if a two term Gaussian was used or a blue line if a single term Gaussian was used. The mean (points) and standard deviation (error bars) calculated via the standard formulas and from the Gaussian fit constants are shown as an orange x or a purple asterisks, respectively.

View Article Online
DOI: 10.1039/D5NR01790D

As shown in figure 2, bimodal distributions of the AM-FM AFM data prevented accurate calculation of sample means and standard deviations when the standard formulas were used. To overcome this issue, as described in supplementary section S3, the mean and standard deviation of substrate AM-FM AFM data was calculated by fitting Gaussians to the data distributions. For individual image statistics, the distribution used for the fit comprised of pixel values from a particular AM-FM AFM image. For overall statistics, the distribution comprised of pixel values from all AM-FM AFM images. The mean and standard deviation calculated from the Gaussian fit represent the most prominent peak of the distribution, corresponding to the most prevalent polymer structure (for example, polymer orientation, tangling, or other topographies) in the substrate. As shown in figure 2, this Gaussian fit method of calculating sample statistics matches the values from the standard formulas if the data distribution is unimodal.

3.2.2 Substrate Properties at AM-FM AFM Measurement Frequencies

Representative AM-FM AFM images of each substrate are shown in figure 3. Poly(HEMA) substrates are shown in figure 3A-C. The two highest concentrations of poly(HEMA) look similar, but have different mechanical properties. The lowest concentration of poly(HEMA), 0.114 mg poly(HEMA) per cm^2 of the substrate's surface, formed clumps rather than a uniform coating on the coverslip (magenta arrows in figure 3A). These clumps were easy to displace with the AFM tip, and prone to sticking to the tip, which occasionally interfered with quantification of E' and $\tan\delta$ (magenta arrows in figure 3B and C).

Representative AM-FM AFM images of pureCol substrates collected with an AC240TSA are shown in figure 3D-F. Figure 7B-D and supplementary figure S12 show representative AM-FM AFM images collected with an RC800PSA. PureCol substrate topography and viscoelasticity varied with GA concentration. Additionally, pureCol substrate topography differed when different cantilevers with different sensitivities to tip/pureCol interactions (already demonstrated in figure 1A and C) were used. For example, interactions between

View Article Online
DOI: 10.1039/D5NR01790D

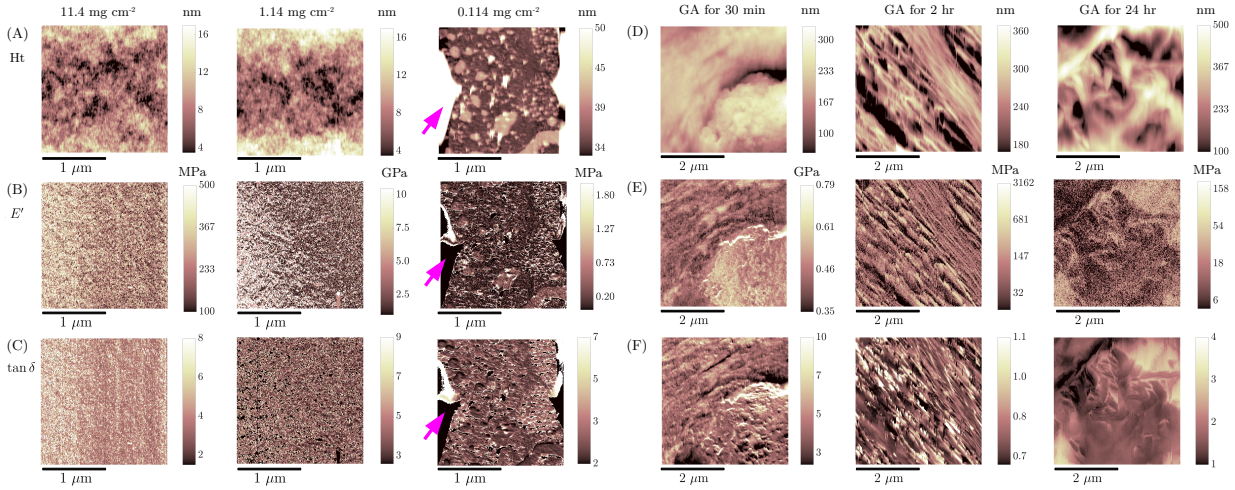

Figure 3: Representative AM-FM AFM images of each substrate. Sample feature height (Ht) is shown in the top row for poly(HEMA) and pureCol substrates (A and D, respectively), storage modulus, E', in the middle row (B and E, respectively), and loss tangent, $\tan\delta$, in the bottom row (C and F, respectively). Poly(HEMA) substrates were synthesized by successively diluting poly(HEMA) in ethanol, depositing the resulting solutions onto glass coverslips, and allowing the substrate to polymerize. The columns in A-C correspond to substrates with 11.4 mg of poly(HEMA) per cm^2 of sample surface area, 1.14 mg poly(HEMA) per cm^2, and 0.114 mg poly(HEMA) per cm^2, respectively. Magenta arrows indicate poly(HEMA) clumps in the 0.114 mg per cm^2 sample that interfered with quantification of E' and $\tan\delta$. PureCol substrates were synthesized by allowing pureCol (collagen I) to polymerize, then crosslinking the collagen with glutaraldehyde (GA) for varying amounts of time. The columns in D-F correspond to substrates crosslinked for 30 minutes, two hours, or 24 hours.

sample hydration shells and an AFM tip can vary with cantilever selection, and affect the tip's ability to image a sample.[154,155]

To quantify the differences in AM-FM AFM images between substrates, figure 4 shows the mean height (surface topography, not substrate thickness), E', and $\tan\delta$ of each substrate. As shown in figure 4A, topography of the 11.4 and 1.14 mg poly(HEMA) per cm^2 substrates was the same ($p = 0.99$). The mean and standard deviation in film height of the 0.114 mg poly(HEMA) per cm^2 substrates were larger than the other poly(HEMA) substrates, meaning the sample exhibited more varied topography. This observation agrees with the fact that large poly(HEMA) clumps surrounded by glass were observed on the 0.114 mg poly(HEMA) per cm^2 substrates, but not substrates with higher poly(HEMA) concentrations (figure 3A).

View Article Online
DOI: 10.1039/D5NR01790D

Poly(HEMA) films are known to uniformly coat the underlying substrate, but decrease in thickness with decreasing poly(HEMA) concentration,[112] until the polymer is sparse enough that clumps form and the film is no longer uniform (figure 3A). The identical topography of the 11.4 mg per cm^2 and 1.14 mg per cm^2 substrates (figure 4A) agrees with the literature observations[112] that poly(HEMA) films are uniform unless the polymer is too sparse.

As shown in figure 4C, E' was highest for the 1.14 mg poly(HEMA) per cm^2 substrates ($p = 0.02$ vs. the 11.4 mg cm^{-2} sample and $p = 0.05$ vs. the 0.114 mg cm^{-2} sample). Since the main difference between each substrate is the thickness of the poly(HEMA) film or clumps[112] on the coverslip, not the poly(HEMA) itself, these results show that film thickness affects E'. The fact that E' increased as the poly(HEMA) film thinned suggests that coverslip glass underlying the poly(HEMA) influenced the measurements, even though the tip did not indent through to the glass. This influence, where an underlying hard substrate alters the tip/sample interaction on thin soft substrates, is referred to as a bottom effect.[156] In such cases, a bottom effect correction should be applied in the contact model.[156] Reliance on the Hertz contact model in AM-FM AFM neglects this correction,[156] likely leading to incorrectly high values of E' for the 1.14 mg per cm^2 substrate, and possibly other poly(HEMA) concentrations. Additionally, the fact that E' of the 0.114 mg poly(HEMA) per cm^2 substrate was closer to that of the 11.4 mg per cm^2 substrate supports the notion that bottom effects are present in poly(HEMA) measurements. Poly(HEMA) clumping in the 1.14 mg poly(HEMA) per cm^2 substrate could have been substantial enough to reduce bottom effects. Furthermore, as shown in figure 4F, $\tan\delta$ was not significantly different between the different poly(HEMA) substrates ($p > 0.2$ for all comparisons). The fact that $\tan\delta$, but not E', is independent of contact mechanics, including bottom effects,[87,107] lends support to the notion that a bottom effect was present in poly(HEMA) E' values. However, expansion of AM-FM AFM's calculation of E' to include a bottom effect correction is beyond the scope of this work. Regardless, cells on substrates with low poly(HEMA) concentrations might be able to probe through the poly(HEMA) to the underlying material. The fact that $\tan\delta$

View Article Online
DOI: 10.1039/D5NR01790D

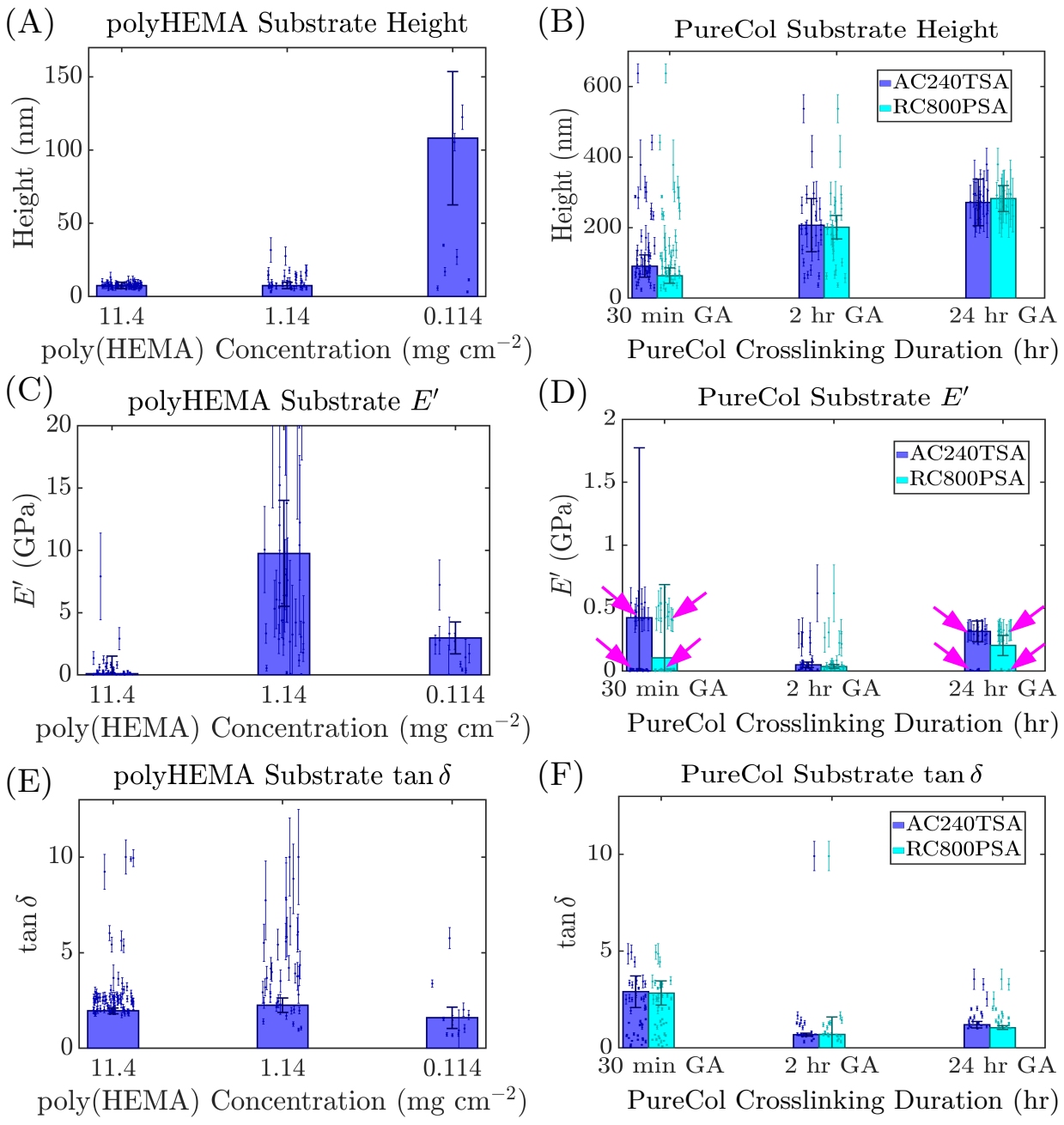

Figure 4: Effect of poly(HEMA) concentration (A, C, and E) and pureCol crosslinking (B, D, and F) on substrate feature height (A,B), storage modulus (E', C,D), and loss tangent ($\tan\delta$, E,F). Bars represent overall mean values, calculated from all measured pixels. Smaller dots with error bars represent the mean values of individual AM-FM AFM images, calculated from all measured pixels within the image. Error bars represent the standard deviation. Metrics were calculated as described in section 3.2.1. Magenta arrows indicate different values of E' within a given substrate.

View Article Online
DOI: 10.1039/D5NR01790D

was not significantly different between the different poly(HEMA) substrates, combined with the likelihood that alterations to E' of poly(HEMA) substrates were due to bottom effects rather than differences in poly(HEMA) viscoelasticity, suggests that poly(HEMA) substrates modulate cell activities by how much cells can probe the underlying substrate through the poly(HEMA) film.

The properties of pureCol substrates varied more than poly(HEMA) substrates. Feature height on the surface of pureCol substrates (figure 4B) increased with increasing GA crosslinking duration ($p < 0.04$ for all comparisons). This trend agrees with previous observations that GA crosslinking increases the diameter of collagen fibers.[122] The increase is likely due to rearrangement of collagen fibrils by crosslinking. For example, consider one immobile polymer and one free polymer. If a single crosslink forms between the immobile polymer and the free polymer, the ends of the free polymer will fluctuate around the crosslink until coming into contact with other locations on the immobile polymer with which another crosslink can form.[7] If a subsequent crosslink forms, motion of the free polymer is even more restricted along the dimensions of the immobile polymer.[7] Eventually, as crosslinks are added, the free polymer will align with the immobile polymer.[7] In other words, polymers are bundled together as crosslinking occurs. With longer exposure to GA, more crosslinks form,[124] resulting in more polymer bundling, thicker fibers, and thus the observed increase in feature height and fiber diameter with crosslinking duration.

Figure 4D shows that E' of pureCol substrates increased with crosslinking duration ($p < 0.01$ for both cantilevers), and the increased crosslink density with longer GA exposure. E' of substrates crosslinked for 30 minutes or 24 hours varied between AM-FM AFM images, as indicated by magenta arrows in figure 4C. Note that the representative E' maps in figure 3E correspond to the lower E' values (lower magenta arrows in figure 4D). This heterogeneity suggests that the amount of GA crosslinking varied locally at the nanoscale. Since the substrates were roughly 0.3 cm thick (supplementary figure S11), the variation in E' is not due to a bottom effect, but due to local variations in pureCol configuration. As shown by

View Article Online
DOI: 10.1039/D5NR01790D

figure 4F, $\tan\delta$ was not significantly different between samples crosslinked for 2 and 24 hours ($p = 0.64$ for RC800PSA cantilevers and $p = 0.10$ for AC240TSA cantilevers). Substrate $\tan\delta$ was higher for samples crosslinked for 30 minutes ($p \leq 0.01$ for both comparisons with both cantilevers). Since $\tan\delta = E''/E'$, this observation demonstrates that crosslinks affect energy storage (E') and dissipation (E'') in collagen substrates differently.

3.2.3 Viscoelastic Behavior of Each Substrate

Literature studies have found that both poly(HEMA)[113,127–131] and collagen I[65–71,132–135] substrates are viscoelastic. However, it is important to verify that the substrates measured in this study are indeed viscoelastic. This validation can be accomplished using AM-FM AFM data to determine whether the sample behaves as a linear viscoelastic material, as previously established.[87] In this determination, $(\tan\delta E')^{-1}$ is plotted against $(E')^{-1}$ for all pixels in a single AM-FM AFM image. If the points are well described by a line, one of the standard models of linear viscoelasticity: the GMM, SLS, KV, or MW model (model details can be found in supplementary section S1), describes the sample's response.[87] If the sample behaves as a GMM, SLS, KV, or MW material, other types of time dependent mechanical responses such as poroelasticity can be neglected, and the sample considered viscoelastic.

Figure 5 and 6 show representative plots of $(\tan\delta E')^{-1}$ against $(E')^{-1}$ from all pixels of a single AM-FM AFM image of each substrate as well as a linear fit to the data. If the linear fit has low RMSE, the sample is a GMM, SLS, MW or KV material, as detailed in section 2.3 and supplementary section S2.2.[87,146] GMM, SLS, MW and KV model details can be found in supplementary section S1. Figure 5 shows example model tests for the three poly(HEMA) substrates. Mean fit metrics for all AM-FM AFM images of the poly(HEMA) substrates can be found in supplementary table S2. Fit metrics for each AM-FM AFM image of the 11.4, 1.14, and 0.114 mg poly(HEMA) per cm^2 substrates can be found in supplementary tables S3, S4, and S5, respectively. The mean ± standard deviation in the RMSE values of the model test fits to each sample were 0.0376 ± 0.0111 for substrates with 11.4 mg poly(HEMA)

View Article Online
DOI: 10.1039/D5NR01790D

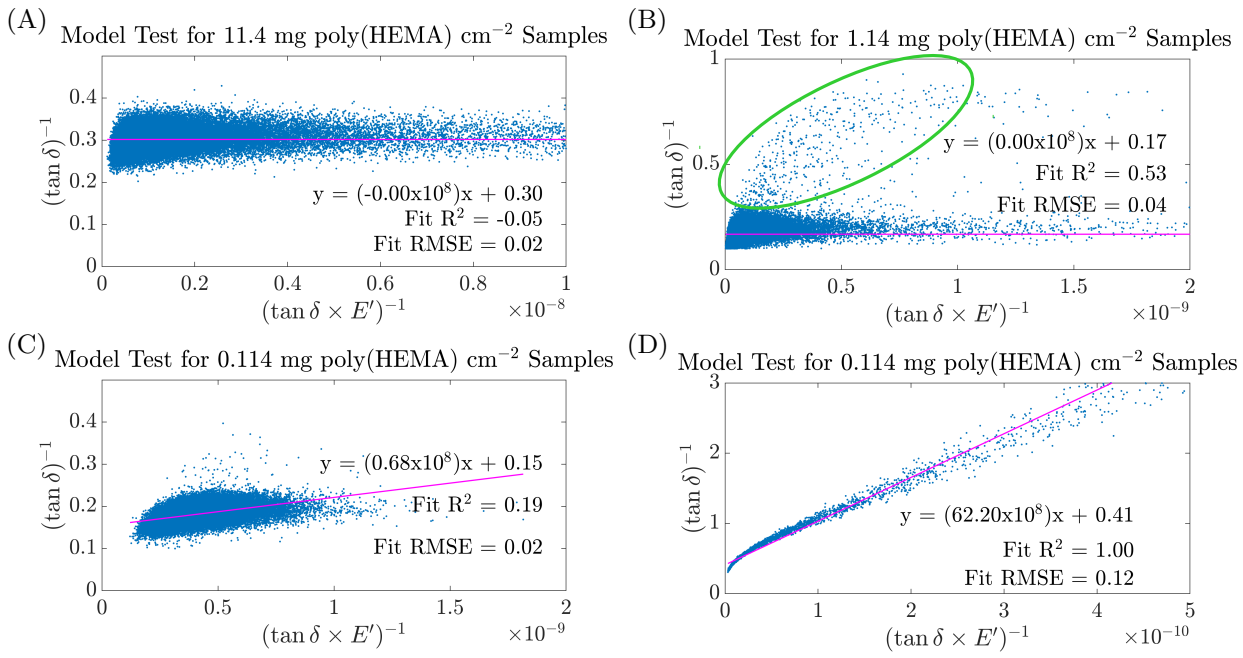

Figure 5: Example model tests for poly(HEMA) substrates. Each plot corresponds to a single AM-FM AFM image. Blue dots represent values from individual pixels of the image. The model test line (equation S21) is shown in magenta. The fit equation, R^2 value, and root mean square error (RMSE) are also shown. Model tests for substrates with 11.4 mg poly(HEMA) per cm^2 of sample surface area and 1.14 mg per cm^2 are shown in (A) and (B), respectively. The green circle in (B) indicates a second material in the sample. Model tests for two different AM-FM AFM images of the 0.114 mg per cm^2 substrate are shown in (C) and (D), to illustrate the variation in model test outcomes for this substrate.

per cm^2, 0.0499 ± 0.0577 for substrates with 1.14 mg poly(HEMA) per cm^2, and 0.1752 ± 0.1395 for substrates with 0.114 mg poly(HEMA) per cm^2, indicating that the data can be approximated by a line, and therefore that poly(HEMA) substrates can be modeled with the MW, KV, SLS, or GMM models. The RMSE values, as well as the standard deviation in RMSE increase as poly(HEMA) concentration decreases. These changes are likely the result of thinning poly(HEMA) film structures and variations in bottom effects on the less concentrated substrates.

Most linear fits had $m \approx 0$ and $b > 0$ (figure 5A and B, supplementary tables S3, S4, and S5), indicating that poly(HEMA) behaves mostly as a MW material. However, some fits exhibited $m > 0$, and a hyperbolic shape (figure 5C and D), indicating that poly(HEMA) also obeys the GMM. In general, $m > 0$ occurred more as poly(HEMA) concentration decreased,

View Article Online
DOI: 10.1039/D5NR01790D

appearing most in substrates with 0.114 mg poly(HEMA) per cm^2. Since the GMM appeared more in substrates with lower poly(HEMA) concentrations, which have the thinnest poly(HEMA) films[112,113] and likely bottom effects (section 3.2.2), it is reasonable to hypothesize that the GMM corresponds to a convolution of the glass and poly(HEMA) or bottom effects. In other words, poly(HEMA) is a MW material, but transitions to a GMM as the poly(HEMA) film thins and becomes more affected by the underlying coverslip. Regardless, these results confirm that the poly(HEMA) substrates in this study are viscoelastic, as expected from the literature.[113,127–131]

Figure 6 shows representative model tests for pureCol substrates. As shown in supplementary table S2, the mean ± standard deviation in RMSE for pureCol substrate measurements performed with an RC800PSA were: 0.22 ± 1.21 for pureCol crosslinked for 30 minutes, 0.05 ± 0.03 for pureCol crosslinked for 2 hours, and 0.03 ± 0.03 for pureCol crosslinked for 24 hours. The mean ± standard deviation in RMSE for measurements performed with an AC240TSA were: 0.31 ± 1.19 for pureCol crosslinked for 30 minutes, 0.17 ± 0.16 for pureCol crosslinked for 2 hours, 0.05 ± 0.02 for pureCol crosslinked for 24 hours. Fit metrics for individual images, as well as the assigned model for the given image can be found in supplementary tables S6, S7, and S8. PureCol substrates crosslinked for 30 minutes had the largest variation in RMSE for both cantilevers. This observation is likely due to the fact that sample mechanics were more heterogeneous in this substrate compared to substrates crosslinked for longer times (see section 3.2.2). Regardless, the low RMSE values confirm that pureCol substrates can be modeled as a GMM or one of the GMM's special cases.

For individual AM-FM AFM images of each pureCol substrate, the linear fits all exhibited a nonzero y-intercept, indicating that the substrates should not be modeled as KV materials. Some fits for pureCol substrates crosslinked for 30 minutes (supplementary table S6) had small slopes, and therefore behaved as MW materials (figure 6A and E). Others (figure 6B and F) had a slope greater than zero, and therefore obeyed the SLS or GMM. Similar outcomes occurred for substrates crosslinked for 2 (see supplementary table S7) or

View Article Online
DOI: 10.1039/D5NR01790D

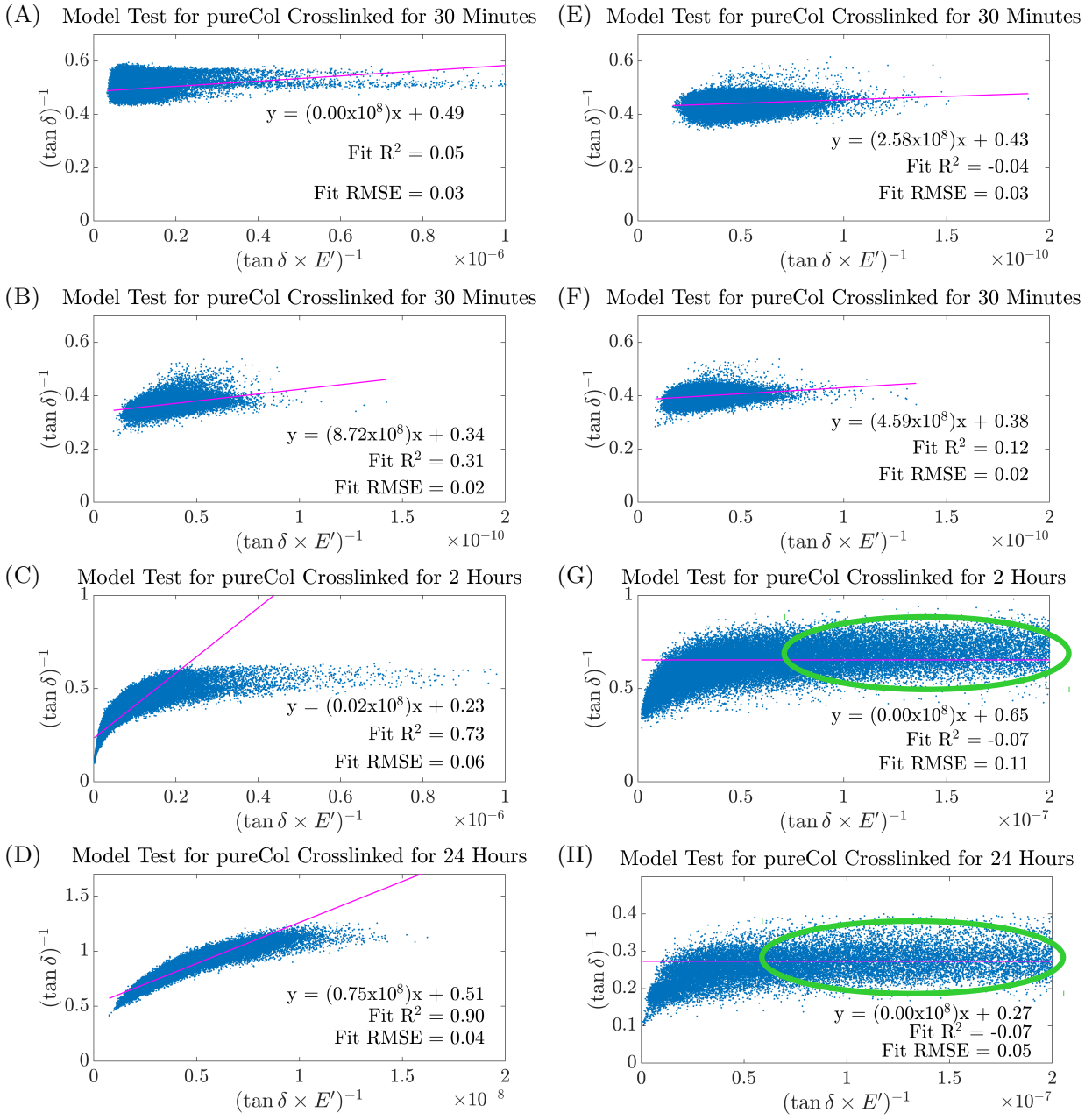

Figure 6: Example model tests for pureCol substrates. Each plot corresponds to a single AM-FM AFM image. Blue dots represent values from individual pixels of the image. The model test line (equation S21) is shown in magenta. The fit equation, R^2 value, and root mean square error (RMSE) are also shown. Model tests for AM-FM AFM data collected with an RC800PSA cantilever are shown in (A)-(D). Similarly, model tests for data collected with an AC240TSA cantilever are shown in (E)-(H). Green circles indicate a Maxwell material (supplementary section S2.2) in the AC240TSA model tests that is not present in the RC800PSA model tests. Representative model tests for pureCol substrates crosslinked for 30 minutes are shown in (A), (B), (E), and (F). Comparisons of (A) with (B) or (E) with (F) show differences in the model test outcome for these substrates. Representative model tests for pureCol substrates crosslinked for 2 hours are shown in (C) and (G). Representative model tests for pureCol substrates crosslinked for 24 hours are shown in (D) and (H).

View Article Online
DOI: 10.1039/D5NR01790D

24 hours (supplementary table S8). Regardless of substrate, plots with a nonzero slope and y-intercept, while well described by a line, exhibited a slightly curved shape, meaning that the GMM is the best model to describe these samples.[87,146]

Of the basic models of linear viscoelasticity, the MW model is best to describe samples that are more fluid.[7,157] Additionally, pureCol substrates are fluid without crosslinking, and substrate fluidity decreases as the number of crosslinks increases (see section 3.1). Furthermore, samples with longer crosslinking duration, and therefore more crosslinks,[124] exhibit MW behavior in the model test less frequently (see supplementary tables S6, S7, and S8). These observations suggest the MW material corresponds to regions of a substrate with less crosslinking, and the GMM material corresponds to regions of the sample with more crosslinking.

Model test outcomes on pureCol substrates varied slightly between RC800PSA and AC240TSA cantilevers. The RMSE values were higher for data collected with the AC240TSA cantilever compared to the RC800PSA, due to increased presence of an additional material (green circles in figure 6) in AC240TSA model tests that was less apparent in RC800PSA model tests. This second material did not exhibit a large slope, and therefore behaved as a MW material. Additionally, the fact that this material was more present in AC240TSA measurements suggests that the material is related to cantilever/sample interactions, rather than the substrate itself. Since AC240TSAs are more sensitive to pureCol surface layers than RC800PSA cantilevers (section 3.1), the additional MW material in the AC240TSA measurements likely corresponds to surface hydration shells, polymer brushes, or similar surface features. Such features are relatively fluid compared to the bulk, and since the MW model is best to describe samples that are more fluid,[7,157] it is reasonable that surface features behave as MW materials.

Together, these results demonstrate that the substrates in this study can be modeled as GMM or MW materials, and are therefore viscoelastic, matching previous literature observations of similar substrates.[65–71,113,127–135] Therefore, the measurements in this paper describe

View Article Online
DOI: 10.1039/D5NR01790D

viscoelasticity, rather than other time dependent responses such as poroelasticity.

3.3 PT-AFM nDMA measurements of Cell Culture Substrates

Representative PT-AFM nDMA measurements of E', E'', and $\tan\delta$ at different points on each cell culture substrate are shown in figure 7. Before these measurements were obtained, several control experiments were necessary to determine whether PT-AFM nDMA measurements could reliably be performed in liquid.[105,107] These controls are detailed in supplementary sections S7-S10, and recommendations for performing PT-AFM nDMA measurements on new samples in liquid based on these tests are detailed in supplementary section S11.

The first control experiment for liquid PT-AFM nDMA, described in supplementary section S7, was performed to evaluate whether hydrodynamic drag[105] would impair PT-AFM nDMA measurements in liquid. Hydrodynamic drag depends on the fluid structure near a sample's surface and could affect the sample and reference measurements differently, thereby introducing artifacts to AFM nDMA measurements.[105] Therefore, to test these effects, a single sample measurement was analyzed against several reference measurements performed at different heights above the sample.[105,107] Hydrodynamic drag affected measurements at some reference heights for particular cantilever/sample pairings. When hydrodynamic drag affected PT-AFM nDMA measurements, discontinuities or oscillations occurred in the measured E', E'', and $\tan\delta$ (supplementary figure S4). When no discontinuities or oscillations were observed, results agreed regardless of reference height (supplementary figure S4). Therefore, for any new sample/cantilever pairing, measurements at different reference heights should be performed to determine the extent of hydrodynamic drag effects for the given system. Reference measurements can be performed at any height where discontinuities and oscillations are not present in the measurements, and where the resulting E', E'', and $\tan\delta$ match those against other reference heights.

The second control experiment, described in supplementary section S8, was performed to ensure that PT-AFM nDMA measurements were performed in the sample's linear viscoelastic

View Article Online
DOI: 10.1039/D5NR01790D

regime by comparing PT-AFM nDMA measurements collected on the sample using different force trigger points. Higher trigger points result in larger sample indentations (details in supplementary section S4). In the linear viscoelastic regime of a sample, E', E'', and $\tan\delta$ will not vary with different trigger points because these properties are independent of indentation depth until the sample is deformed outside of the sample's linear viscoelastic regime.[7] As shown in supplementary figures S5-S7, the linear viscoelastic regime varied between samples, and even different points on the same sample. However, a trigger point of 8 nN was in the linear viscoelastic regime of all samples. Higher trigger points occasionally also fell in the linear viscoelastic regime. Therefore, for any new sample, the linear viscoelastic regime of the sample should be determined by performing sample measurements with different indentation depths.

The third control experiment (supplementary section S9) tested whether the AFM cantilever affects PT-AFM nDMA results by comparing measurements obtained with RC800PSA and AC240TSA cantilevers. While k' and k'' are extensive properties,[106,107,158] and therefore expected to change with different cantilevers, $\tan\delta$ is intensive and independent of contact geometry[106,107,158] and should therefore be the same regardless of cantilever. As shown in supplementary figure S8, the cantilever did not alter the measured $\tan\delta$, meaning that PT-AFM nDMA is robust to different cantilevers.

The final control experiment (supplementary section S10) was performed to test the limits of PT-AFM nDMA. As detailed in section 3.1, certain samples may be too soft and fluid to obtain PT-AFM nDMA measurements. Also described in section 3.1, PT-AFM nDMA may be difficult to perform on samples with strong surface effects, such as surface polymer brushes. To test this hypothesis, a hydrogel synthesized from polydimethylsiloxane (PDMS) was measured by PT-AFM nDMA in liquid. The surface of PDMS hydrogels behaves differently from the bulk due to interfacial differences in the concentration of loose polymer chains and resulting alterations in bulk vs. surface gel swelling and properties.[159] These differences cause surface effects that influence bulk property measurements in AFM nanoindentation

View Article Online
DOI: 10.1039/D5NR01790D

experiments.[159] The reference measurement in PT-AFM nDMA may be unable to account for alterations to cantilever motion due to such effects, since the reference must be obtained when not in contact with the sample, and therefore cannot be collected at the interface. As shown in supplementary figure S9, and discussed in supplementary section S10, the PDMS interface shifted cantilever phase during sample measurements, and thereby rendered the measurements negative and unphysical regardless of reference measurement height. Therefore, PT-AFM nDMA in liquid will not work on samples with unusual interfacial dynamics or with surface polymer brushes because such surfaces influence cantilever motion in a manner that cannot be accounted for by the reference measurement. However, it may be possible to work around such limitations in the future by selecting a cantilever that is less sensitive to such interactions, measuring the sample dry, or using polymer physics models to add correction factors to PT-AFM nDMA calculations. Regardless, these controls show that, for many samples, PT-AFM nDMA can be used to quantify nanoscale sample viscoelasticity in air[107] as well as liquid.

3.3.1 PT-AFM nDMA Measurements at Different Points on poly(HEMA) Substrates

PT-AFM nDMA requires larger indentations than AM-FM AFM[77,106,107] and thus can only be performed on thicker samples (details in supplementary section S5.1). As stated in methods section 2.4.1, sample indentations ranged between 100 nm and 600 nm during PT-AFM nDMA measurements. These indentations constitute roughly 0.01% of pureCol sample thickness and roughly 1%, 10%, and 100% of the 11.4, 1.14, and 0.1 mg poly(HEMA) per cm^2 substrate thicknesses. These percentages are high for lower poly(HEMA) concentrations. Additionally, even the AM-FM AFM measurements of substrates with lower poly(HEMA) concentrations, with much smaller sample indentations,[77] were affected by the underlying glass. Therefore, PT-AFM nDMA was performed only on the 11.4 mg poly(HEMA) per cm^2 substrate. Representative PT-AFM nDMA measurements of E', E'', and $\tan\delta$ of the 11.4

View Article Online
DOI: 10.1039/D5NR01790D

mg poly(HEMA) per cm^2 substrate are shown in figure 7A. The Hertz model was used to calculate PT-AFM nDMA E' and E'' in order to keep the contact model consistent between AM-FM AFM, which solely uses the Hertz model,[76,86] and PT-AFM nDMA (as described in section 2.4.2).

The shape and magnitude of poly(HEMA) $\tan\delta$ measured by PT-AFM nDMA matches those detailed in table 1 and supplementary section S12, and thereby agrees with macroscale

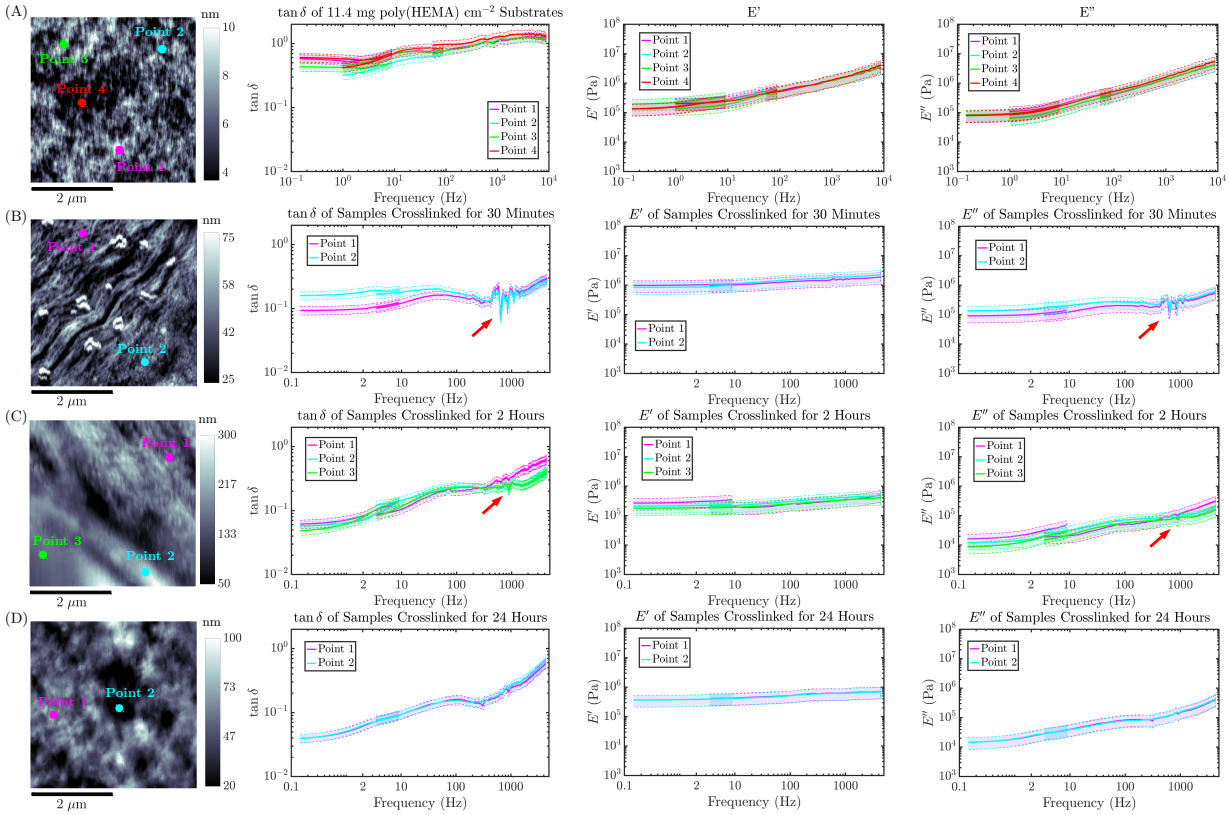

Figure 7: PT-AFM nDMA measurements at different points on cell culture substrates. PT-AFM nDMA was performed on poly(HEMA) substrates with 11.4 mg poly(HEMA) per cm^2 (A), and pureCol substrates crosslinked with glutaraldehyde for 30 minutes (B), two hours (C), or 24 hours (D). A topography image of the substrate, with the location of each PT-AFM nDMA measurement is shown in the left column. The measured loss tangent ($\tan\delta$) is shown in the second column. Storage and loss moduli, E' and E'', calculated from PT-AFM nDMA measurements by applying the Hertz contact model are shown in the third and fourth columns, respectively. Red arrows indicate measurement artifacts introduced by resonances between the cantilever and sample, possibly from tip interactions with loose collagen polymers in the substrate. These measurements are representative of measurements from two biological replicates of the substrate.

View Article Online
DOI: 10.1039/D5NR01790D

literature measurements of poly(HEMA) substrates[127] as well as composite poly(HEMA) acrylamide substrates.[128] E' and E'', calculated by applying the Hertz contact model to measured PT-AFM nDMA k' and k'', have the expected shape, and are on the order of 10^5 Pa, which agrees with the higher end of the 10^3-10^5 Pa range expected from the literature,[127,128] and matches that of substrates made only of poly(HEMA).[127] However, it is important to acknowledge that, based on AM-FM AFM measurements (section 3.2.2), a bottom effect correction and, due to the relatively deep sample indentations during PT-AFM nDMA, a different contact model may be more appropriate to represent the tip/sample interaction than the Hertz model. PT-AFM nDMA measurements of $\tan\delta$, E', and E'' did not vary with position on the sample. This observation agrees with AM-FM AFM observations that the mechanical properties of the 11.4 mg poly(HEMA) per cm^2 sample were homogeneous.

3.3.2 PT-AFM nDMA Measurements at Different Points on pureCol Substrates

PT-AFM nDMA measurements of pureCol substrates were performed using both RC800PSA and AC240TSA cantilevers. Both cantilevers obtained similar results, as detailed in supplementary section S9. Since RC800PSA cantilevers were less sensitive to pureCol surface layers than AC240TSA cantilevers (see section 3.1 and 3.2.2), only PT-AFM nDMA measurements obtained using RC800PSA cantilevers are presented here, but are representative of measurements obtained with AC240TSA cantilevers. PT-AFM nDMA measurements were performed in at least two positions on the surface of each pureCol substrate. The shape and magnitude of pureCol $\tan\delta$ measured by PT-AFM nDMA matches those detailed in table 1 and supplementary section S12, and thereby agree with macroscale literature values for pureCol and other collagen substrates.[67,122,132–135,140–142]

The Hertz contact model[145] was used to calculate E' and E'' of pureCol substrates in order to ensure the same contact model as AM-FM AFM's calculation of E' (see section 2.4.2). E' and E'' of pureCol substrates measured by PT-AFM nDMA had the expected shape, but were on the order of 10^5 - 10^6 Pa and 10^4 - 10^5 Pa, respectively. Both are

View Article Online
DOI: 10.1039/D5NR01790D

three orders of magnitude higher than the expected 10^2 - 10^3 Pa for E', and 10^1 - 10^2 Pa for E'' from most of the literature,[67,122,132–135,139–141] and one to two orders of magnitude lower than the 10^7 - 10^8 Pa for E' and 10^6 - 10^7 Pa for E'' reported in one study.[142] This difference between PT-AFM nDMA measurements and literature E' and E'' could be due to scaling behavior, since PT-AFM nDMA was performed at the nanoscale, while literature measurements[67,122,132–135,139–141] were performed at the macroscale.[160] Nanoscale moduli can sometimes be several orders of magnitude higher than macroscale moduli, as a result of the natural scaling behavior of polymers.[160] Additionally, since the cantilever exhibits a tetrahedral tip geometry, not spherical as assumed in the Hertz model,[145] the samples are viscoelastic, and indentation depths are deep in PT-AFM nDMA, the Hertz contact model is likely not the most accurate model of the tip/sample contact. Changing the contact model may resolve some of the discrepancy between PT-AFM nDMA and literature measurements. However, other contact models are not investigated in this study because AM-FM AFM relies on the Hertz model,[76,86] and the Hertz model must therefore also be applied to PT-AFM nDMA measurements to ensure that results from each technique can be compared.

The fact that the GMM or MW models apply to pureCol substrates (section 3.2.3) can be exploited to determine whether the offset in PT-AFM nDMA E' and E'' compared to the literature is due to scaling behavior or contact model effects by allowing comparison of E' at low measurement frequencies (f) against elastic moduli from indentation experiments. For GMM materials, as $\omega = 2\pi f \to 0$, $E' \to E_c$ (supplementary equation S14) and $E'' \to 0$ (supplementary equation S15). In nanoindentation experiments, indentation speeds are slow, meaning that the measured elastic modulus (E) corresponds to sample behavior at low f, where $E = E_c = E'$.[106,107] Nanoscale collagen E in liquid is on the order of 10^5 - 10^6 Pa calculated by applying the Oliver-Pharr model to nanoindentation measurements,[161] 10^6 Pa calculated by applying the Hertz model with a bottom effect correction to nanoindentation measurements,[162] 10^8 Pa using optical tweezers,[163] and 10^6 Pa using AFM bending measurements (contact model not stated).[164] These nanoscale moduli agree with the measured E'

View Article Online
DOI: 10.1039/D5NR01790D

in PT-AFM nDMA, in spite of varying contact models, and are roughly three to four orders of magnitude higher than the macroscale rheology measurements in the literature. This is the same offset between PT-AFM nDMA and literature measurements, and is independent of contact model. Therefore, collagen DMA at the nanoscale is likely three to four orders of magnitude higher than macroscale control measurements due to scaling behavior.

Together, the fact that all curve shapes and $\tan\delta$ measurements agree with the literature demonstrates that the operating principles of PT-AFM nDMA do not interfere with measurements in liquid. Furthermore, in spite of employing the Hertz model, the magnitude offsets in E' and E'' are most likely due to scaling behavior, not incorrect contact model selection.

Representative PT-AFM nDMA measurements of pureCol substrates crosslinked with GA for 30 minutes are shown in figure 7B. Two points on the sample were measured. The first measurement was performed on a spot with aligned fibrils. The second was performed on a spot without fibrils. E' was the same for both points. For frequencies less than 100 Hz, E'' was lower in the spot with fibrils. Therefore, $\tan\delta$ at frequencies less than 100 Hz was also lower for the spot containing fibrils. The fact that E' was the same in both points of the sample is likely related to sample crosslinking, which would restrict movement of collagen polymers when the substrate was deformed,[126] regardless of the position measured. Values of E'' and $\tan\delta$ were lower for fibrils at frequencies less than 100 Hz. Therefore, fibrils, and regions of the substrate which contain fibrils, do not dissipate as much energy as regions without fibrils, likely due to alterations in polymer orientation and increased confinement of collagen monomers.

Bundling of collagen into fibrils can alter a multitude of polymer properties, including collagen hydration and electrical properties.[165–167] For example, the electrical properties of collagen can be affected by the topography of collagen structures, and play an important role in determining the properties of structures arising from collagen.[165–167] Collagen fibrils posses two axes of electric polarization, one in a longitudinal direction (along the length) of

View Article Online
DOI: 10.1039/D5NR01790D

the fiber, and one in an axial direction (perpendicular to the length of the molecule) along the fiber.[165] When collagen fibrils and fibers align, electric polarization of the resulting structures is maintained.[166] Additionally, randomly oriented collagen deposition can cancel some of the electric polarization of collagen structures.[167] Structures arising from aligned collagen fibrils maintain electric polarization of the fibrils, while structures of randomly oriented collagen may or may not do the same.[165–167] Therefore, it is reasonable to hypothesize that the electrical properties of pureCol substrates, and any resulting hydration shells or other features that depend on electrostatic interactions, are spatially heterogeneous depending on the orientation of collagen molecules in any given region of the sample, and alterations to energy dissipation in different regions of the substrate relate to alterations in the electric polarization, hydration, and intermolecular interactions within these regions as a result of altered collagen topography.

Representative PT-AFM nDMA measurements of pureCol substrates crosslinked with GA for 2 hours are shown in figure 7C. Three points were probed on the sample. The first measurement was performed on a small fiber, with many fibrils distributed over the fiber's surface. The second measurement was performed on a larger fiber, without the small fibrils over the surface. The third measurement was performed on an even larger fiber on the sample. E' and E'' did not vary with position on the sample for frequencies less than 1,000 Hz. At 1,000 Hz, E' and E'' of the first point increased slightly compared to the others. Similarly, $\tan\delta$ of the first point also increased compared to the other points at frequencies above 1,000 Hz. Therefore, fibers where collagen fibrils do not completely incorporate themselves into the fiber (point one in figure 7C) exhibit altered energy storage and dissipation at high frequencies, compared to fibers where the constituent fibrils are fully incorporated. This observation is potentially due to increased freedom of movement for fibrils that are only partially incorporated into fibers. Regardless, some spatial heterogeneity is present in the mechanical properties at particular frequencies of pureCol substrates crosslinked for 2 hours. Additionally, since two of the three points measured by PT-AFM nDMA exhibited similar

View Article Online
DOI: 10.1039/D5NR01790D

mechanical responses, less spatial variation in substrate viscoelasticity may be present than in samples crosslinked for 30 minutes (figure 7B).

Measurements of pureCol samples crosslinked for 30 minutes (figure 7B) and 2 hrs (figure 7C) exhibited fluctuations around 1,000 Hz (red arrows in figure 7B and C) due to resonance between the tip and sample, not sample properties. Such resonance could emerge from a number of interactions. However, most of the measurement curve was unaffected by the resonance at 1,000 Hz, and since behavior at 1,000 Hz was not a focus in this article, the artifacts did not negatively impact measurement results. If desired, resonance effects can be eliminated by applying additional smoothing or using a different cantilever to perform PT-AFM nDMA measurements.

Representative PT-AFM nDMA measurements of pureCol substrates crosslinked with GA for 24 hours are shown in figure 7D. Two points were probed on the sample. The first measurement was performed on a region of clumped collagen on the substrate. The second measurement was performed on a point between collagen clumps. The measured E', E'', and $\tan\delta$ did not vary between the two points. The lack of variation in the mechanical properties of pureCol substrates crosslinked for 24 hours is likely related to the crosslinking in the sample. With more crosslinks, movement of collagen polymers within the substrate would be restricted, thereby limiting spatial heterogeneity in the mechanical properties.[126]

3.4 Substrate Comparisons

Next, the different substrates were compared by averaging PT-AFM nDMA and AM-FM AFM measurements of each substrate. AM-FM AFM E'' was calculated by modeling the sample as a GMM (determined from the model tests, section 3.2.3), calculating GMM material constants as previously described,[87,146] and substituting these constants into supplementary equation S12. The GMM, and not MW model was used to calculate AM-FM AFM E'' because, as detailed in section 3.2.3, figures 5 and 6, and supplementary tables S2-S8, all substrates could be modeled as GMM or MW materials. Since MW materials are special

View Article Online
DOI: 10.1039/D5NR01790D

cases of the GMM,[7,9,146,168] the GMM is the most applicable model for all substrates. Figure 8A-C respectively show the mean E', E'', and $\tan\delta$ over the measured frequencies for all substrates measured by both AM-FM AFM and PT-AFM nDMA.

Sample relaxation time as a function of frequency was calculated using principles of the GMM. As described in supplementary section S1, the GMM can be thought of as N different SLSs connected in parallel.[87,169] The nth arm of the GMM has a relaxation time τ_n. Each of the N SLSs in the GMM has resonance frequency $f_n = 1/\tau_n$.[169] Therefore the nth SLS in a GMM contributes most to E', E'', and $\tan\delta$ when the arm is excited by a stimulus with frequency $f = 1/\tau_n$,[169] meaning that the GMM's mechanical response at a particular frequency can be modeled by the SLS representing the dominant, resonating arms of the GMM at the particular excitation frequency.[168] It is therefore possible to calculate $\tau_r(f)$ of the sample by recalling that, for the SLS, $E' = E_c + \tau_r\omega E''$ (supplementary equation S11). Therefore, τ_r can be calculated from PT-AFM nDMA E' and E'' via equation 6.

$$\tau_r(f) = \frac{E'(f) - E_c}{2\pi f E''(f)} \tag{6}$$

The value of E_c is the value of E' for PT-AFM nDMA measurements at low frequencies (see supplementary equation S14). While E', E_c, and E'' are calculated from AFM measurements by applying contact models, the geometric contribution of the contact to each cancels by taking the ratio of $[E'(f) - E_c]/E''(f)$ in equation 6. Therefore, as with $\tan\delta$,[87,107] τ_r calculated in this manner is also independent of contact geometry. At AM-FM AFM measurement frequencies, τ_r can be calculated by applying similar principles, as previously published.[87,146] Mean relaxation time as a function of frequency for each substrate is shown in figure 8D.

As shown in figure 8, AM-FM AFM values align with PT-AFM nDMA values, demonstrating that each measurement technique agrees with the other. E' and E'' (figure 8A and B) of all substrates increased with increasing frequency. A sharper increase in each modulus corresponding to the glass or similar transition,[157,168] started between 10^3 and 10^4 Hz for

View Article Online
DOI: 10.1039/D5NR01790D

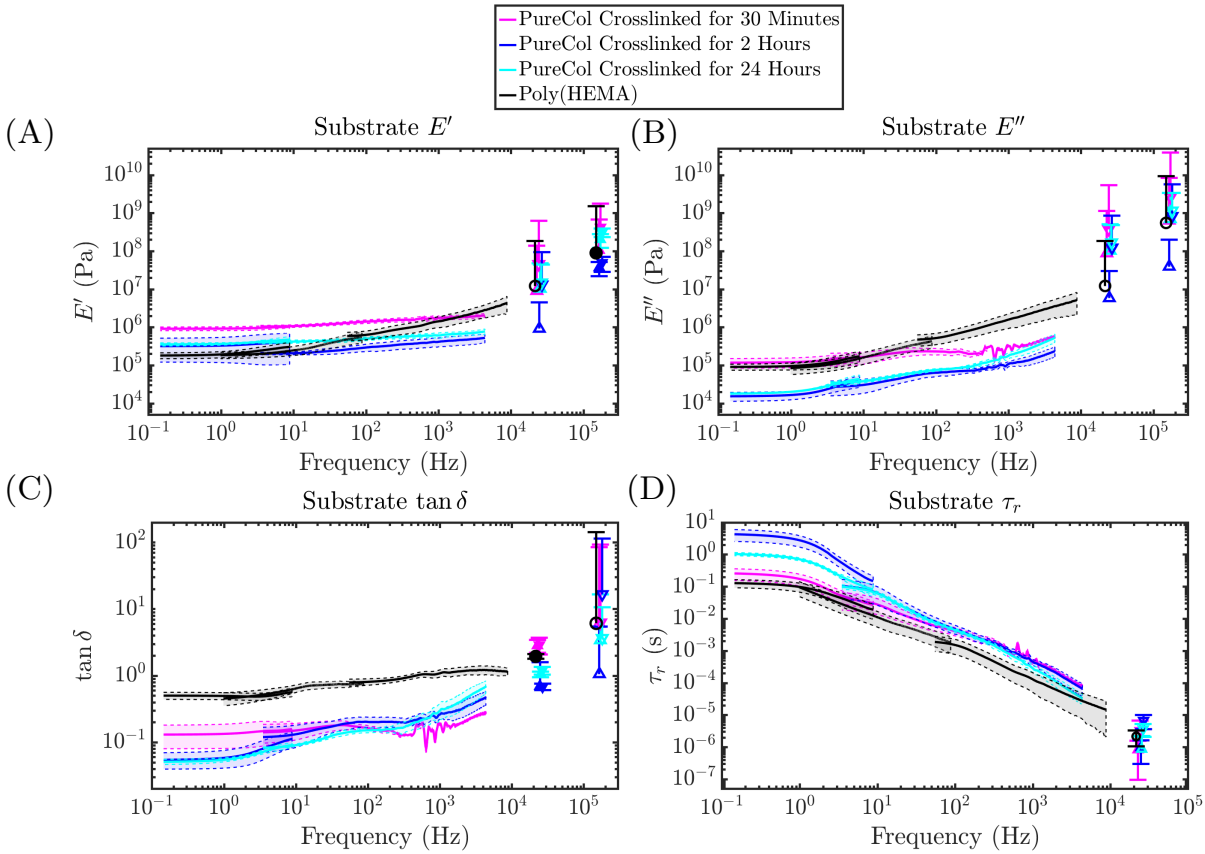

Figure 8: Comparison of substrate viscoelasticity. Measurements of pureCol substrates crosslinked with GA for 30 minutes (magenta), 2 hours (blue), and 24 hours (cyan), in addition to a poly(HEMA) substrate at a concentration of 11.4 mg poly(HEMA) per cm^2 of substrate surface area (black) are shown. The mean value of all PT-AFM nDMA measurements (lines), as well as AM-FM AFM measurements (points), are shown for each substrate. For AM-FM AFM measurements, triangles pointing down represent measurements of pureCol substrates obtained with an AC240TSA, triangles pointing up represent pureCol measurements obtained with an RC800PSA, and circles represent AM-FM AFM measurements of poly(HEMA) substrates with 11.4 mg poly(HEMA) per cm^2 of sample surface area. Shading with dotted lines represents the standard deviation of PT-AFM nDMA measurements. Error bars represent the standard deviation of AM-FM AFM measurements. Filled markers represent AM-FM AFM measurements. Open markers represent values calculated from AM-FM AFM measurements as previously described.[87,146]

View Article Online
DOI: 10.1039/D5NR01790D

pureCol substrates and around 10 Hz for poly(HEMA) substrates. In spite of the fact that the glass transition of poly(HEMA) substrates began around 10 Hz, AM-FM AFM measurements of E' and E'' are similar for poly(HEMA) and pureCol substrates. Therefore, the glass transition is broader for poly(HEMA) than for pureCol.

AM-FM AFM model tests of poly(HEMA) substrates (figure 5) demonstrated that poly(HEMA) behaves as a MW material, but can behave as a GMM as the result of effects from the glass underlying the poly(HEMA). For MW materials, E' and $E'' \sim 0$ at low frequencies, and increase as frequency increases (see supplementary equation S5-S6). However, poly(HEMA) E' and E'' are nonzero at 0.1 Hz. This behavior is more consistent with the GMM, which has a nonzero E' at low frequencies and a gradual increase in E' and E'' with frequency (details in supplementary section S1, equations S14-S16).[87,168] While this observation could be due to a bottom effect,[156] it is also possible that $E' \to 0$ for frequencies lower than 0.1 Hz, the lowest frequency measured in this article. The latter is the most likely case because literature measurements of poly(HEMA) exhibit similar shapes to the PT-AFM nDMA measurements for $f > 0.001$ Hz.[127,128] AM-FM AFM model tests of pureCol substrates (figure 6) demonstrated that these substrates behave according to the MW or GMM models. This observation is supported by PT-AFM nDMA measurements, which show trends in E' and E'' characteristic of the GMM (details in supplementary section S1, equations S14-S16).[87,168] Therefore, PT-AFM nDMA measurements and AM-FM AFM model tests are in agreement about the viscoelastic behavior of these substrates. Additionally, collagen substrates have previously been modeled as MW materials, but exhibit rheology curves consistent with GMM behavior at $f > 0.1$ Hz,[133] agreeing with the combined AM-FM AFM and PT-AFM nDMA measurements in this study.

Of the pureCol substrates, pureCol crosslinked for 30 minutes exhibited the highest E' and E'' in both AM-FM AFM (figure 4B) and PT-AFM nDMA (figure 8). As detailed in supplementary section S12, previous literature reported that increased GA crosslinking can increase[122,140,141] or decrease[142] both the storage and loss moduli, depending on measurement

View Article Online
DOI: 10.1039/D5NR01790D

preloading conditions.[67,126] PT-AFM nDMA trends agree with those observed on samples with moduli on the order of 10^6 - 10^8 Pa measured in liquid,[142] and are therefore not unreasonable. GA crosslinking modulates viscoelasticity of collagen substrates by restricting the movement of fibrils within the substrate, rather than by directly altering the mechanical properties of the fibrils.[126] With less crosslinking, polymer movement is only partially restricted, and collagen chains have more freedom to deform, interact with one another, and interact with hydration layers. In other words, there are more ways to store and dissipate energy in response to deformation in substrates with less crosslinking. As crosslink density increases, the relatively lower E' and E'' likely arise due to increased restriction of collagen fibril movement limiting interactions that store and dissipate energy.

E' of poly(HEMA) substrates was comparable to pureCol substrates crosslinked for 2 or 24 hours. Poly(HEMA) E'' was comparable to pureCol substrates crosslinked for 30 minutes. Therefore, poly(HEMA) exhibited a higher ratio of E''/E' than pureCol samples. As shown in figure 8C, $\tan\delta$ of poly(HEMA) substrates was roughly one order of magnitude higher than that of pureCol substrates. Alterations in pureCol $\tan\delta$ with frequency varied between the substrates. In samples crosslinked for 30 minutes, $\tan\delta$ was constant for frequencies less than 10^3 Hz, then began to increase. For substrates crosslinked 2 and 24 hours, $\tan\delta$ steadily increased with increasing frequency.

Unlike E' and E'', literature measurements of $\tan\delta$ with different GA crosslinking agree and demonstrate that $\tan\delta$ is 1.2 - 4 fold lower for substrates with more crosslinking.[122,140–142] PT-AFM nDMA results showed that $\tan\delta$ of pureCol substrates crosslinked for 30 minutes was roughly three times higher than that of substrates with longer crosslinking durations at measurement frequencies less than 10 Hz, and are therefore in agreement with the literature. Additionally, the observation that E', E'', and $\tan\delta$ were similar in substrates crosslinked for 2 and 24 hours agrees with literature measurements that also found more GA crosslinking decreases the difference between rheology curves.[122,140–142] Therefore, PT-AFM nDMA measurements of crosslinking effects agree with those expected from the literature (see table

View Article Online
DOI: 10.1039/D5NR01790D

1 and supplementary section S12 for more details on literature expectations).

The value of $\tau_r(f)$ at high frequencies is similar for all substrates. At frequencies less than 10 Hz, $\tau_r(f)$ is roughly one order of magnitude shorter for poly(HEMA) and pureCol substrates crosslinked for 30 minutes than for pureCol substrates crosslinked for 2 or 24 hours. Since the differences between E' of these two groups are smaller than the differences in E'' (figure 8A and B), the longer τ_r at low frequencies are the result of greater changes in energy dissipation relative to energy storage between the two groups. For most measurement frequencies, τ_r is longer in pureCol substrates crosslinked for 2 or 24 than substrates crosslinked for 30 minutes. This trend of longer relaxation times with more GA crosslinking agrees with previous literature.[67]

At frequencies less than 1 Hz, τ_r of pureCol substrates crosslinked in GA for 2 hours is closest to that of pureCol substrates crosslinked for 24 hours. Between 1 and 100 Hz, τ_r of pureCol substrates crosslinked for 2 hours transitions to values similar to those of pureCol crosslinked for 30 minutes. At frequencies around 300 Hz, all three pureCol substrates exhibit similar τ_r. Substrates with 2 hour GA crosslinking have an intermediate distribution of τ_r between the other pureCol substrates, likely because the crosslinking in this sample is also the intermediate of the pureCol substrates.

4 Discussion

The results of this study demonstrate that the measured poly(HEMA) and pureCol substrates are viscoelastic and can be modeled with the GMM or MW models (section 3.2.3), that substrate viscoelasticity varies locally at the nanoscale (section 3.2 and 3.3.1), and that substrate viscoelasticity varies between materials and with different amounts of crosslinking (section 3.4). PT-AFM nDMA measurements agreed with AM-FM AFM measurements (figure 8). Additionally, PT-AFM nDMA measurements agreed with literature controls on measurement curve shape and changes due to crosslinking (section 3.3.1 and figure 8). Fur-

View Article Online
DOI: 10.1039/D5NR01790D

thermore, the order of magnitude of all $\tan\delta$ measurements and poly(HEMA) E' and E'' measurements agreed with the literature (section 3.3.1 and figure 8). While pureCol E' and E'' were three orders of magnitude higher than macroscale literature controls, comparison of these values to nanoindentation measurements in the literature suggests that this offset is due to scaling behavior between nanoscale and macroscale measurements, and is therefore not a failure of PT-AFM nDMA. Together, these results demonstrate that PT-AFM nDMA can be successfully employed in liquid environments to quantify nanoscale viscoelastic behavior in biologically relevant conditions over a broad and continuous range of frequencies.

This work highlights several factors to consider when performing PT-AFM nDMA in liquid. First, the technique will not work in liquid on samples with unusual interfacial dynamics or with surface polymer brushes because such surfaces influence cantilever motion in a manner that cannot be accounted for by the reference measurement. While it may be possible to work around such limitations in the future by selecting a cantilever that is less sensitive to interfacial interactions, measuring the sample dry, or using polymer physics models to add correction factors to PT-AFM nDMA calculations, this investigation is left to future work. Second, when performing PT-AFM nDMA, each new cantilever/sample pairing should undergo similar control measurements to those described in section 3.3 and supplementary sections S7 - S11. Specifically, hydrodynamic drag effects should be evaluated by comparing the sample measurement to reference measurements obtained at different heights from the sample. The linear viscoelastic regime of the sample should be determined by obtaining sample measurements at different indentation depths. An optional control is to test cantilever effects by performing measurements with different cantilevers. Third, $\tan\delta$ and τ_r measurements are robust to contact model because the geometric features of the tip/sample contact for these properties cancel for both quantities. Therefore, $\tan\delta$ and τ_r are the most robust PT-AFM nDMA measurement properties (section 2.3 and 8). The measured E' and E'' are calculated by applying a contact model (section 2.3), and effects of tip/sample interaction geometry must therefore be considered for these properties.

View Article Online
DOI: 10.1039/D5NR01790D

4.1 Contact Model Effects in PT-AFM nDMA Calculations of E' and E''

Throughout PT-AFM nDMA measurements in this article, the Hertz contact model was used to calculate E' and E'' from PT-AFM nDMA's measured k' and k'', even though the tetrahedral tip geometry, viscoelastic samples, and deep sample indentations violate Hertz model assumptions.[9,145] Use of the Hertz model in this article was a deliberate choice in order to emphasize and assess the effect of a widely used contact model[9,145] on PT-AFM nDMA, even if model assumptions are violated by the technique.

In spite of the fact that the Hertz contact model was employed to calculate PT-AFM nDMA E' and E'', continuous measurement curves with the expected shape based on macroscale rheology measurements were still obtained, meaning that curve shape is independent of contact model. This result is expected because many contact models shift k' and k'' by a constant (the value of which is calculated by the contact model), and therefore move the curve up or down, but do not alter curve shape.[107] Therefore, if an incorrect contact model is used, PT-AFM nDMA can still inform relative comparisons of E' and E'' across locations on a single sample or different samples, just not the exact magnitude of each quantity. If the only objective is to compare whether one curve is higher than another, then this comparison can be made even when an incorrect contact model is applied. However, more care must be applied to select the appropriate contact model if E' and E'' order of magnitude is of particular interest to the given study.

It is important to emphasize that $\tan\delta$ is independent of contact model, because the geometric factors in E' and E'' cancel when taking the ratio of the two.[87,107] Similarly, because the geometric factors of the tip/sample contact cancel in the calculation of τ_r (see section 3.4), time responses of a sample can be analyzed even if the wrong contact model is applied. If the best contact model for the given tip/sample interaction is unknown, calculation of E' and E'' can be avoided, and $\tan\delta$ can still be considered alone. Alternatively, as in this article, the Hertz model can be employed with multiple controls for the measured value of

View Article Online
DOI: 10.1039/D5NR01790D

E' and E'' to ascertain whether magnitude shifts, if present, are due to scaling or contact model effects. Furthermore, the Hertz model is widely used in AFM.[9,75,76] If the Hertz model is used in place of a more accurate contact model, PT-AFM nDMA measurements can be combined with and compliment measurements from other techniques such as AM-FM AFM, as described in section 3.4.

4.2 Possible Link between Substrate Properties and Cell Behaviors

The AFM measurements of cell culture substrates in this article reflected several important features of these substrates. Investigation of poly(HEMA) substrates demonstrated that less concentrated poly(HEMA) substrates may not be uniform films, and that the activities of cells on poly(HEMA) relate to how much of the underlying glass the cells can sense through the poly(HEMA). Therefore, to obtain a full picture of what cells sense on poly(HEMA) substrates, it is likely necessary to consider the convoluted poly(HEMA)/underlying material properties. To test this hypothesis in the future, poly(HEMA) films can be prepared on substrates to which cells do not attach, for example, agar. If cell attachment to the poly(HEMA), and any resulting cell activities, are altered compared to poly(HEMA) on glass, this observation would support the notion that cells sense a convolution of the material underlying poly(HEMA) as well as the poly(HEMA) itself.

Cells probe their substrate at low frequencies.[170] Therefore, the mechanical properties of substrates at low frequencies are particularly relevant to what cells sense on the substrate.[170] At low frequencies, pureCol substrates crosslinked with GA for 2 or 24 hours exhibited longer relaxation times, by roughly one order of magnitude, than poly(HEMA) substrates and pureCol substrates crosslinked for 30 minutes. While both energy storage and dissipation were different between the slow and fast τ substrates, alterations to the relaxation times were the result of greater differences in energy dissipation than differences in energy storage between the slow and fast substrates. Since $E'' = 0$ if a substrate has no viscosity,[7,9,146,168] these observations demonstrate that it is essential to measure substrate

View Article Online
DOI: 10.1039/D5NR01790D

viscoelasticity, rather than treating substrates as purely elastic, to obtain a full picture of how a substrate's properties affect cell behavior.

The different substrate time responses at low frequencies (figure 8D) have interesting implications for cell behaviors on the substrates. It is already hypothesized that shorter τ_r promotes ECM deposition and remodeling, as well as differentiation of cells within the substrate, and reduces proliferation and migration.[61] Longer τ_r promotes the opposite.[60] On collagen substrates, cells proliferate more,[171,172] perform less ECM remodeling and contraction,[171,172] and differentiate less[171] on substrates crosslinked with GA. Cells also exhibit increased seeding efficiency (meaning more cells attach to the substrate when they are seeded onto the substrate), and infiltrate the substrate faster (show increased invasion and migration) with more GA crosslinking.[172] Therefore, cells on highly crosslinked collagen substrates exhibit the same behaviors as cells on substrates with longer time responses.[60,61,171,172,172] Additionally, the pureCol findings in this article show that substrates with more GA crosslinking exhibit longer time responses, supporting the hypothesis that longer substrate time responses promote cell attachment, proliferation, and migration (invasion and infiltration), and hinder ECM remodeling and differentiation.

Poly(HEMA) measurements further support the notion that substrate time responses relate to cell behaviors. The inability of cells to attach to poly(HEMA)[112] supports the hypothesis that shorter substrate relaxation times result in decreased cell attachment. Reduced DNA synthesis,[112] reduced cell activation,[136] reduced cell migration, and reduced cell signaling[113] by cells on poly(HEMA) coincide with the hypothesized effects of shortened response times.[61] Additionally, it is interesting to note that poly(HEMA) promoted the formation of multiple nuclei within malignant melanoma cells.[113] In tissues, cells with multiple nuclei (polykaryons) normally form as the result of immune, muscle, or placental cell differentiation processes.[173,174] Therefore, the formation of polykaryons on poly(HEMA) could suggest that these cells underwent some type of differentiation process. If this is the case, this observation also agrees with shorter time responses promoting cell differentiation.

View Article Online
DOI: 10.1039/D5NR01790D

It is interesting to note that poly(HEMA) and pureCol crosslinked for 30 minutes had similar time responses at low frequencies. In spite of the similar substrate time responses, cells attach and spread on pureCol,[171,172] but not to poly(HEMA).[112] Therefore, other properties of the substrate also play an important role in cell behavior. For example, the hydrophilic nature of poly(HEMA) plays an important role in preventing cell attachment.[113] Additionally, it is already known that poly(HEMA) alters the mechanical properties of cells, likely by altering cytoskeleton dynamics.[136] Together, these observations suggest that chemical properties, and likely other properties such as electrical, and possibly magnetic properties, of a substrate alter the effects of substrate time responses by altering cell mechanics, and thereby the sensitivity of the cells to substrate mechanics. The different physical properties of a substrate likely combine to regulate cell mechanics, and thereby cell activities. Regardless, the results in this article combined with the literature describing cell behaviors on similar substrates build upon previous work[60,61] suggesting that shorter substrate time responses promote ECM remodeling and differentiation and hinder cell attachment, proliferation, and migration (invasion and infiltration), while the opposite is true for longer substrate time responses.

5 Conclusions

In this study, PT-AFM nDMA, a novel AFM technique that allows nanoscale viscoelasticity characterization over a broad and continuous frequency range,[107] was applied to samples in liquid for the first time. The technique successfully and accurately characterized the viscoelasticity of cell culture substrates, and synergized with AM-FM AFM measurements of the same substrate. In liquid, it is important to consider hydrodynamic drag and sample heterogeneity, as detailed in this article (see supplementary sections S7-S11, main text section 3.3, and details from the initial PT-AFM nDMA publication[107]). Regardless, the measurements in this article demonstrate that, in addition to air,[107] PT-AFM nDMA can

View Article Online
DOI: 10.1039/D5NR01790D

also be performed in liquid environments. In particular, such capabilities allow greater characterization of biological samples. Comparing cell behaviors on similar substrates reported in the literature to PT-AFM nDMA measurements of the cell culture substrates in this study supports the hypothesis that substrates with longer time responses at low measurement frequencies promote cell attachment, proliferation, and migration (invasion and infiltration), while shorter substrate time responses promote ECM remodeling and differentiation. Further testing of this hypothesis, and application of PT-AFM nDMA to biological samples will enhance understanding of how cell and tissue mechanics dictate cell behavior.

6 Author Contributions

C.E.A. performed all PT-AFM nDMA measurements, poly(HEMA) and pureCol sample preparation, data analysis, and data visualization. C.E.A. also designed the experiments. A.R.P. helped design and advise the control experiments to test whether PT-AFM nDMA could be performed in liquid environments. Y.Z. synthesized the PDMS substrates and shadowed the PDMS PT-AFM nDMA measurements. C.E.A. and S.C. wrote the paper with input from the other authors. S.L.W. and S.C. supervised the work.

7 Data Availability

Data will be made available upon request to the corresponding author.

8 Conflicts of Interest

The authors have no conflicts of interest to declare.

View Article Online
DOI: 10.1039/D5NR01790D

Acknowledgement

The authors thank Dr. Jacob Seifert Kineast for the helpful discussions, Dr. Steven Tucker for his feedback, and Dr. Núria Gavara for her feedback and insights. Additionally, the authors thank George F. Edick for introducing C.E.A. to the substrates in this article and suggesting poly(HEMA) as a substrate.

Supporting Information Available

The following files are available free of charge.

- Supplementary Material PDF: A PDF containing supplementary explanations of viscoelasticity, AFM technique principles, and data analysis, details of control experiments when performing PT-AFM nDMA in liquid, a review of the literature measurements used as controls in this study, supplementary figures, and supplementary tables.

References

(1) Weaver, V. M. Cell and tissue mechanics: the new cell biology frontier. *Molecular Biology of the Cell 28*, 1815–1818.

(2) Bonnans, C.; Chou, J.; Werb, Z. Remodelling the extracellular matrix in development and disease. *Nature Reviews Molecular Cell Biology 15*, 786–801.

(3) Brindley, D.; Moorthy, K.; Lee, J.-H.; Mason, C.; Kim, H.-W.; Wall, I. Bioprocess Forces and Their Impact on Cell Behavior: Implications for Bone Regeneration Therapy. *Journal of Tissue Engineering* 620247.

(4) Tee, S.-Y.; Bausch, A. R.; Janmey, P. A. The mechanical cell. *Current Biology 19*, R745–R748.

View Article Online
DOI: 10.1039/D5NR01790D

(5) Humphrey, J. D.; Dufresne, E. R.; Schwartz, M. A. Mechanotransduction and extracellular matrix homeostasis. *Nature Reviews Molecular Cell Biology 15*, 802–812.

(6) Vogel, V.; Sheetz, M. Local force and geometry sensing regulate cell functions. *Nature Reviews Molecular Cell Biology 7*, 265–275.

(7) Doi, M. *Soft matter physics*, first edition ed.; Oxford University Press, 2013; OCLC: ocn857650756.

(8) Seifert, J. In vivo dynamic AFM mapping of viscoelastic properties of the primary plant cell wall. 2018.

(9) Popov, V. L.; Heß, M.; Willert, E. *Handbook of Contact Mechanics: Exact Solutions of Axisymmetric Contact Problems*; Springer Berlin Heidelberg, 2019.

(10) Klein, E. A.; Yin, L.; Kothapalli, D.; Castagnino, P.; Byfield, F. J.; Xu, T.; Levental, I.; Hawthorne, E.; Janmey, P. A.; Assoian, R. K. Cell-Cycle Control by Physiological Matrix Elasticity and In Vivo Tissue Stiffening. *Current Biology 19*, 1511–1518.

(11) Wang, H.-B.; Dembo, M.; Wang, Y.-L. Substrate flexibility regulates growth and apoptosis of normal but not transformed cells. *American Journal of Physiology-Cell Physiology 279*, C1345–C1350.

(12) Kong, H. J.; Polte, T. R.; Alsberg, E.; Mooney, D. J. FRET measurements of cell-traction forces and nano-scale clustering of adhesion ligands varied by substrate stiffness. *Proceedings of the National Academy of Sciences 102*, 4300–4305.

(13) Koyama, H.; Raines, E. W.; Bornfeldt, K. E.; Roberts, J. M.; Ross, R. Fibrillar collagen inhibits arterial smooth muscle proliferation through regulation of Cdk2 inhibitors. *Cell 87*, 1069–1078.

(14) Huang, S.; Ingber, D. E. The structural and mechanical complexity of cell-growth control. *Nature Cell Biology 1*, E131–E138.

View Article Online
DOI: 10.1039/D5NR01790D

(15) Engler, A. J.; Sen, S.; Sweeney, H. L.; Discher, D. E. Matrix Elasticity Directs Stem Cell Lineage Specification. *Cell 126*, 677–689.

(16) Fu, J.; Wang, Y.-K.; Yang, M. T.; Desai, R. A.; Yu, X.; Liu, Z.; Chen, C. S. Mechanical regulation of cell function with geometrically modulated elastomeric substrates. *Nature Methods 7*, 733–736.

(17) Kilian, K. A.; Bugarija, B.; Lahn, B. T.; Mrksich, M. Geometric cues for directing the differentiation of mesenchymal stem cells. *Proceedings of the National Academy of Sciences 107*, 4872–4877.

(18) Karnik, S. K. A critical role for elastin signaling in vascular morphogenesis and disease. *Development 130*, 411–423.

(19) Brooke, B. S.; Bayes-Genis, A.; Li, D. Y. New insights into elastin and vascular disease. *Trends in Cardiovascular Medicine 13*, 176–181.

(20) Montell, D. J. Morphogenetic Cell Movements: Diversity from Modular Mechanical Properties. *Science 322*, 1502–1505.

(21) Solon, J.; Kaya-Çopur, A.; Colombelli, J.; Brunner, D. Pulsed Forces Timed by a Ratchet-like Mechanism Drive Directed Tissue Movement during Dorsal Closure. *Cell 137*, 1331–1342.

(22) Trappmann, B.; Gautrot, J. E.; Connelly, J. T.; Strange, D. G. T.; Li, Y.; Oyen, M. L.; Cohen Stuart, M. A.; Boehm, H.; Li, B.; Vogel, V.; Spatz, J. P.; Watt, F. M.; Huck, W. T. S. Extracellular-matrix tethering regulates stem-cell fate. *Nature Materials 11*, 642–649.

(23) Viswanathan, P.; Ondeck, M. G.; Chirasatitsin, S.; Ngamkham, K.; Reilly, G. C.; Engler, A. J.; Battaglia, G. 3D surface topology guides stem cell adhesion and differentiation. *Biomaterials 52*, 140–147.

View Article Online
DOI: 10.1039/D5NR01790D

(24) Task, K.; D'Amore, A.; Singh, S.; Candiello, J.; Jaramillo, M.; Wagner, W. R.; Kumta, P.; Banerjee, I. Systems level approach reveals the correlation of endoderm differentiation of mouse embryonic stem cells with specific microstructural cues of fibrin gels. *Journal of The Royal Society Interface 11*, 20140009–20140009.

(25) Discher, D. E.; Mooney, D. J.; Zandstra, P. W. Growth Factors, Matrices, and Forces Combine and Control Stem Cells. *Science 324*, 1673–1677.

(26) Lecuit, T.; Lenne, P.-F. Cell surface mechanics and the control of cell shape, tissue patterns and morphogenesis. *Nature Reviews Molecular Cell Biology 8*, 633–644.

(27) Charras, G.; Sahai, E. Physical influences of the extracellular environment on cell migration. *Nature Reviews Molecular Cell Biology 15*, 813–824.

(28) Wei, S. C.; Fattet, L.; Tsai, J. H.; Guo, Y.; Pai, V. H.; Majeski, H. E.; Chen, A. C.; Sah, R. L.; Taylor, S. S.; Engler, A. J.; Yang, J. Matrix stiffness drives epithelial-mesenchymal transition and tumour metastasis through a TWIST1-G3BP2 mechanotransduction pathway. *Nature Cell Biology 17*, 678–688.

(29) Peyton, S. R.; Putnam, A. J. Extracellular matrix rigidity governs smooth muscle cell motility in a biphasic fashion. *Journal of Cellular Physiology 204*, 198–209.

(30) Pelham, R. J.; Wang, Y. l. Cell locomotion and focal adhesions are regulated by substrate flexibility. *Proceedings of the National Academy of Sciences of the United States of America 94*, 13661–13665.

(31) Plotnikov, S.; Pasapera, A.; Sabass, B.; Waterman, C. Force Fluctuations within Focal Adhesions Mediate ECM-Rigidity Sensing to Guide Directed Cell Migration. *Cell 151*, 1513–1527.

(32) Brammer, K. S.; Oh, S.; Gallagher, J. O.; Jin, S. Enhanced cellular mobility guided by TiO2 nanotube surfaces. *Nano Letters 8*, 786–793.

View Article Online
DOI: 10.1039/D5NR01790D

(33) Lo, C.-M.; Wang, H.-B.; Dembo, M.; Wang, Y.-l. Cell Movement Is Guided by the Rigidity of the Substrate. *Biophysical Journal 79*, 144–152.

(34) Miteva, D. O.; Rutkowski, J. M.; Dixon, J. B.; Kilarski, W.; Shields, J. D.; Swartz, M. A. Transmural Flow Modulates Cell and Fluid Transport Functions of Lymphatic Endothelium. *Circulation Research 106*, 920–931.

(35) Shields, J. D.; Fleury, M. E.; Yong, C.; Tomei, A. A.; Randolph, G. J.; Swartz, M. A. Autologous Chemotaxis as a Mechanism of Tumor Cell Homing to Lymphatics via Interstitial Flow and Autocrine CCR7 Signaling. *Cancer Cell 11*, 526–538.

(36) Yeung, T.; Georges, P. C.; Flanagan, L. A.; Marg, B.; Ortiz, M.; Funaki, M.; Zahir, N.; Ming, W.; Weaver, V.; Janmey, P. A. Effects of substrate stiffness on cell morphology, cytoskeletal structure, and adhesion. *Cell Motility and the Cytoskeleton 60*, 24–34.

(37) Yoshigi, M.; Hoffman, L. M.; Jensen, C. C.; Yost, H. J.; Beckerle, M. C. Mechanical force mobilizes zyxin from focal adhesions to actin filaments and regulates cytoskeletal reinforcement. *The Journal of Cell Biology 171*, 209–215.

(38) Iyer, K.; Pulford, S.; Mogilner, A.; Shivashankar, G. Mechanical Activation of Cells Induces Chromatin Remodeling Preceding MKL Nuclear Transport. *Biophysical Journal 103*, 1416–1428.

(39) Cavalcanti-Adam, E. A.; Micoulet, A.; Blümmel, J.; Auernheimer, J.; Kessler, H.; Spatz, J. P. Lateral spacing of integrin ligands influences cell spreading and focal adhesion assembly. *European Journal of Cell Biology 85*, 219–224.

(40) Totsukawa, G.; Yamakita, Y.; Yamashiro, S.; Hartshorne, D. J.; Sasaki, Y.; Matsumura, F. Distinct roles of ROCK (Rho-kinase) and MLCK in spatial regulation of MLC phosphorylation for assembly of stress fibers and focal adhesions in 3T3 fibroblasts. *The Journal of Cell Biology 150*, 797–806.

View Article Online
DOI: 10.1039/D5NR01790D

(41) Kaunas, R.; Nguyen, P.; Usami, S.; Chien, S. Cooperative effects of Rho and mechanical stretch on stress fiber organization. *Proceedings of the National Academy of Sciences of the United States of America 102*, 15895–15900.

(42) Girard, P. R.; Nerem, R. M. Shear stress modulates endothelial cell morphology and F-actin organization through the regulation of focal adhesion-associated proteins. *Journal of Cellular Physiology 163*, 179–193.

(43) Chrzanowska-Wodnicka, M.; Burridge, K. Rho-stimulated contractility drives the formation of stress fibers and focal adhesions. *The Journal of Cell Biology 133*, 1403–1415.

(44) Riveline, D.; Zamir, E.; Balaban, N. Q.; Schwarz, U. S.; Ishizaki, T.; Narumiya, S.; Kam, Z.; Geiger, B.; Bershadsky, A. D. Focal contacts as mechanosensors: externally applied local mechanical force induces growth of focal contacts by an mDia1-dependent and ROCK-independent mechanism. *The Journal of Cell Biology 153*, 1175–1186.

(45) Choquet, D.; Felsenfeld, D. P.; Sheetz, M. P. Extracellular matrix rigidity causes strengthening of integrin-cytoskeleton linkages. *Cell 88*, 39–48.

(46) Colombelli, J.; Besser, A.; Kress, H.; Reynaud, E. G.; Girard, P.; Caussinus, E.; Haselmann, U.; Small, J. V.; Schwarz, U. S.; Stelzer, E. H. K. Mechanosensing in actin stress fibers revealed by a close correlation between force and protein localization. *Journal of Cell Science 122*, 1665–1679.

(47) Gaus, K.; Le Lay, S.; Balasubramanian, N.; Schwartz, M. A. Integrin-mediated adhesion regulates membrane order. *The Journal of Cell Biology 174*, 725–734.

(48) Altrock, E.; Muth, C. A.; Klein, G.; Spatz, J. P.; Lee-Thedieck, C. The significance of integrin ligand nanopatterning on lipid raft clustering in hematopoietic stem cells. *Biomaterials 33*, 3107–3118.

View Article Online
DOI: 10.1039/D5NR01790D

(49) Bissell, M. J.; Aggeler, J. Dynamic reciprocity: how do extracellular matrix and hormones direct gene expression? *Progress in Clinical and Biological Research 249*, 251–262.

(50) Chiquet, M.; Gelman, L.; Lutz, R.; Maier, S. From mechanotransduction to extracellular matrix gene expression in fibroblasts. *Biochimica et Biophysica Acta (BBA) - Molecular Cell Research 1793*, 911–920.

(51) Verma, S. K.; Lal, H.; Golden, H. B.; Gerilechaogetu, F.; Smith, M.; Guleria, R. S.; Foster, D. M.; Lu, G.; Dostal, D. E. Rac1 and RhoA differentially regulate angiotensinogen gene expression in stretched cardiac fibroblasts. *Cardiovascular Research 90*, 88–96.

(52) Gawlak, G.; Tian, Y.; O'Donnell, J. J.; Tian, X.; Birukova, A. A.; Birukov, K. G. Paxillin mediates stretch-induced Rho signaling and endothelial permeability *via* assembly of paxillin-p42/44MAPK-GEF-H1 complex. *The FASEB Journal 28*, 3249–3260.

(53) Sako, Y. Barriers for lateral diffusion of transferrin receptor in the plasma membrane as characterized by receptor dragging by laser tweezers: fence versus tether. *The Journal of Cell Biology 129*, 1559–1574.

(54) Kusumi, A.; Nakada, C.; Ritchie, K.; Murase, K.; Suzuki, K.; Murakoshi, H.; Kasai, R. S.; Kondo, J.; Fujiwara, T. Paradigm shift of the plasma membrane concept from the two-dimensional continuum fluid to the partitioned fluid: high-speed single-molecule tracking of membrane molecules. *Annual Review of Biophysics and Biomolecular Structure 34*, 351–378.

(55) O'Callaghan, C. J.; Williams, B. Mechanical strain-induced extracellular matrix production by human vascular smooth muscle cells: role of TGF-beta(1). *Hypertension (Dallas, Tex.: 1979) 36*, 319–324.

View Article Online
DOI: 10.1039/D5NR01790D

(56) Tamada, M.; Sheetz, M. P.; Sawada, Y. Activation of a Signaling Cascade by Cytoskeleton Stretch. *Developmental Cell 7*, 709–718.

(57) Winer, J. P.; Oake, S.; Janmey, P. A. Non-Linear Elasticity of Extracellular Matrices Enables Contractile Cells to Communicate Local Position and Orientation. *PLoS ONE 4*, e6382.

(58) Sawhney, R. K.; Howard, J. Slow local movements of collagen fibers by fibroblasts drive the rapid global self-organization of collagen gels. *The Journal of Cell Biology 157*, 1083–1092.

(59) Balaban, N. Q.; Schwarz, U. S.; Riveline, D.; Goichberg, P.; Tzur, G.; Sabanay, I.; Mahalu, D.; Safran, S.; Bershadsky, A.; Addadi, L.; Geiger, B. Force and focal adhesion assembly: a close relationship studied using elastic micropatterned substrates. *Nature Cell Biology 3*, 466–472.

(60) Charrier, E. E.; Pogoda, K.; Wells, R. G.; Janmey, P. A. Control of cell morphology and differentiation by substrates with independently tunable elasticity and viscous dissipation. *Nature Communications 9*, 449.

(61) Chaudhuri, O.; Gu, L.; Klumpers, D.; Darnell, M.; Bencherif, S. A.; Weaver, J. C.; Huebsch, N.; Lee, H.-p.; Lippens, E.; Duda, G. N.; Mooney, D. J. Hydrogels with tunable stress relaxation regulate stem cell fate and activity. *Nature Materials 15*, 326–334.

(62) Bennett, M.; Cantini, M.; Reboud, J.; Cooper, J. M.; Roca-Cusachs, P.; Salmeron-Sanchez, M. Molecular clutch drives cell response to surface viscosity. *Proceedings of the National Academy of Sciences 115*, 1192–1197.

(63) Vining, K. H.; Mooney, D. J. Mechanical forces direct stem cell behaviour in development and regeneration. *Nature Reviews. Molecular Cell Biology* **2017**, *18*, 728–742.

View Article Online
DOI: 10.1039/D5NR01790D

(64) Umut Ozcan, M.; Ocal, S.; Basdogan, C.; Dogusoy, G.; Tokat, Y. Characterization of frequency-dependent material properties of human liver and its pathologies using an impact hammer. *Medical Image Analysis 15*, 45–52.

(65) Amis, E. J.; Carriere, C. J.; Ferry, J. D.; Veis, A. Effect of pH on collagen flexibility determined from dilute solution viscoelastic measurements. *International Journal of Biological Macromolecules 7*, 130–134.

(66) Meghezi, S.; Couet, F.; Chevallier, P.; Mantovani, D. Effects of a Pseudophysiological Environment on the Elastic and Viscoelastic Properties of Collagen Gels. *International Journal of Biomaterials 2012*, 1–9.

(67) Nam, S.; Hu, K. H.; Butte, M. J.; Chaudhuri, O. Strain-enhanced stress relaxation impacts nonlinear elasticity in collagen gels. *Proceedings of the National Academy of Sciences 113*, 5492–5497.

(68) Sasaki, N. In *Viscoelasticity - From Theory to Biological Applications*; De Vicente, J., Ed.; InTech.

(69) Shen, Z.; Kahn, H.; Ballarini, R.; Eppell, S. Viscoelastic Properties of Isolated Collagen Fibrils. *Biophysical Journal 100*, 3008–3015.

(70) Xu, B.; Li, H.; Zhang, Y. Understanding the viscoelastic behavior of collagen matrices through relaxation time distribution spectrum. *Biomatter* **2013**, *3*, e24651.

(71) Sopakayang, R.; De Vita, R.; Kwansa, A.; Freeman, J. W. Elastic and viscoelastic properties of a type I collagen fiber. *Journal of Theoretical Biology 293*, 197–205.

(72) Gonzalez-Molina, J.; Zhang, X.; Borghesan, M.; Mendonça da Silva, J.; Awan, M.; Fuller, B.; Gavara, N.; Selden, C. Extracellular fluid viscosity enhances liver cancer cell mechanosensing and migration. *Biomaterials 177*, 113–124.

View Article Online
DOI: 10.1039/D5NR01790D

(73) Adam, J. A.; Gulati, S.; Hirsa, A. H.; Bonocora, R. P. Growth of microorganisms in an interfacially driven space bioreactor analog. *npj Microgravity 6*, 11.

(74) Butt, H.-J.; Cappella, B.; Kappl, M. Force measurements with the atomic force microscope: Technique, interpretation and applications. *Surface Science Reports* **2005**, *59*, 1–152.

(75) Efremov, Y. M.; Okajima, T.; Raman, A. Measuring viscoelasticity of soft biological samples using atomic force microscopy. *Soft Matter* **2020**, *16*, 64–81.

(76) Labuda, A.; Kocuń, M.; Meinhold, W.; Walters, D.; Proksch, R. Generalized Hertz model for bimodal nanomechanical mapping. *Beilstein Journal of Nanotechnology* **2016**, *7*, 970–982.

(77) Kocun, M.; Labuda, A.; Meinhold, W.; Revenko, I.; Proksch, R. Fast, High Resolution, and Wide Modulus Range Nanomechanical Mapping with Bimodal Tapping Mode. *ACS Nano* **2017**, *11*, 10097–10105.

(78) Solares, S. D.; Chawla, G. Frequency response of higher cantilever eigenmodes in bimodal and trimodal tapping mode atomic force microscopy. *Measurement Science and Technology* **2010**, *21*, 125502.

(79) Haugstad, G. *Atomic force microscopy: understanding basic modes and advanced applications*; John Wiley & Sons, 2012.

(80) García, R. Dynamic atomic force microscopy methods. *Surface Science Reports* **2002**, *47*, 197–301.

(81) Castro García, R. *Amplitude modulation atomic force microscopy*; 2011; OCLC: 1180151008.

(82) Al-Rekabi, Z.; Contera, S. Multifrequency AFM reveals lipid membrane mechanical

View Article Online
DOI: 10.1039/D5NR01790D

properties and the effect of cholesterol in modulating viscoelasticity. *Proceedings of the National Academy of Sciences* **2018**, *115*, 2658–2663.

(83) Benaglia, S.; Gisbert, V. G.; Perrino, A. P.; Amo, C. A.; Garcia, R. Fast and high-resolution mapping of elastic properties of biomolecules and polymers with bimodal AFM. *Nature Protocols* **2018**, *13*, 2890–2907.

(84) Proksch, R.; Yablon, D. G. Loss tangent imaging: Theory and simulations of repulsive-mode tapping atomic force microscopy. *Applied Physics Letters* **2012**, *100*, 073106.

(85) Proksch, R.; Kocun, M.; Hurley, D.; Viani, M.; Labuda, A.; Meinhold, W.; Bemis, J. Practical loss tangent imaging with amplitude-modulated atomic force microscopy. *Journal of Applied Physics* **2016**, *119*, 134901.

(86) Herruzo, E. T.; Garcia, R. Theoretical study of the frequency shift in bimodal FM-AFM by fractional calculus. *Beilstein Journal of Nanotechnology* **2012**, *3*, 198–206.

(87) Adam, C. E.; Piacenti, A. R.; Waters, S. L.; Contera, S. Enhancing nanoscale viscoelasticity characterization in bimodal atomic force microscopy. *Soft Matter* **2024**, *20*, 7457–7470.

(88) Kolluru, P. V.; Eaton, M. D.; Collinson, D. W.; Cheng, X.; Delgado, D. E.; Shull, K. R.; Brinson, L. C. AFM-Based Dynamic Scanning Indentation (DSI) Method for Fast, High-Resolution Spatial Mapping of Local Viscoelastic Properties in Soft Materials. *Macromolecules* **2018**, *51*, 8964–8978.

(89) Pittenger, B.; Osechinskiy, S.; Yablon, D.; Mueller, T. Nanoscale DMA with the Atomic Force Microscope: A New Method for Measuring Viscoelastic Properties of Nanostructured Polymer Materials. *The Journal of The Minerals, Metals & Materials Society (JOM)* **2019**, *71*, 3390–3398.

View Article Online
DOI: 10.1039/D5NR01790D

(90) Igarashi, T.; Fujinami, S.; Nishi, T.; Asao, N.; Nakajima,; Ken, Nanorheological Mapping of Rubbers by Atomic Force Microscopy. *Macromolecules* **2013**, *46*, 1916–1922.

(91) Nguyen, H. K.; Ito, M.; Fujinami, S.; Nakajima, K. Viscoelasticity of Inhomogeneous Polymers Characterized by Loss Tangent Measurements Using Atomic Force Microscopy. *Macromolecules* **2014**, *47*, 7971–7977.

(92) Arai, M.; Ueda, E.; Liang, X.; Ito, M.; Kang, S.; Nakajima, K. Viscoelastic maps obtained by nanorheological atomic force microscopy with two different driving systems. *Japanese Journal of Applied Physics* **2018**, *57*, 08NB08.

(93) Ueda, E.; Liang, X.; Ito, M.; Nakajima, K. Dynamic Moduli Mapping of Silica-Filled Styrene-Butadiene Rubber Vulcanizate by Nanorheological Atomic Force Microscopy. *Macromolecules* **2019**, *52*, 311–319.

(94) Mahaffy, R. E.; Shih, C. K.; MacKintosh, F. C.; Käs, J. Scanning Probe-Based Frequency-Dependent Microrheology of Polymer Gels and Biological Cells. *Phys. Rev. Lett.* **2000**, *85*, 880.

(95) Alcaraz, J.; Buscemi, L.; Grabulosa, M.; Trepat, X.; Fabry, B.; Farré, R.; Navajas, D. Microrheology of Human Lung Epithelial Cells Measured by Atomic Force Microscopy. *Biophysical Journal 84*, 2071–2079.

(96) Mahaffy, R. E.; Park, S.; Gerde, E.; Käs, J.; Shih, C. K. Quantitative Analysis of the Viscoelastic Properties of Thin Regions of Fibroblasts Using Atomic Force Microscopy. *Biophysical Journal* **2004**, *86*, 1777–1793.

(97) Rigato, A.; Miyagi, A.; Scheuring, S.; Rico, F. High-Frequency Microrheology Reveals Cytoskeleton Dynamics in Living Cells. *Nature Physics* **2017**, *13*, 771–775.

(98) Marc Schächtele, M.; Hänel, E.; Schäffer, T. E. Resonance Compensating Chirp Mode

View Article Online
DOI: 10.1039/D5NR01790D

for Mapping the Rheology of Live Cells by High-Speed Atomic Force Microscopy. *Applied Physics Letters* **2018**, *113*, 093701.

(99) Lherbette, M.; dos Santos, A.; Hari-Gupta, Y.; Fili, N.; Toseland, C. P.; Schaap, I. A. T. Atomic Force Microscopy Micro-Rheology Reveals Large Structural Inhomogeneities in Single Cell-Nuclei. *Scientific Reports* **2017**, *7*, 8116.

(100) Nia, H. T.; Han, L.; Li, Y.; Ortiz, C.; Grodzinsky, A. Poroelasticity of Cartilage at the Nanoscale. *Biophysical Journal* **2011**, *101*, 2304–2313.

(101) Nia, H. T.; Bozchalooi, I. S.; Li, Y.; Youcef-Toumi, K.; Ortiz, C.; Grodzinsky, A. High-Bandwidth AFM-Based Rheology Reveals That Cartilage Is Most Sensitive to High Loading Rates at Early Stages of Impairment. *Biophysical Journal* **2013**, *104*, 1529–1537.

(102) Nia, H. T.; Han, L.; Bozchalooi, I. S.; Roughley, P.; Youcef-Toumi, K.; Grodzinsky, A.; Ortiz, C. Aggrecan Nanoscale Solid-Fluid Interactions Are a Primary Determinant of Cartilage Dynamic Mechanical Properties. *ACS Nano* **2015**, *9*, 2614–2625.

(103) Azadi, M.; Nia, H. T.; Gauci, S. J.; Ortiz, C.; Fosang, A. J.; Grodzinsky, A. J. Wide Bandwidth Nanomechanical Assessment of Murine Cartilage Reveals Protection of Aggrecan Knock-in Mice from Joint-Overuse. *Journal of Biomechanics* **2016**, *49*, 1634–1640.

(104) Nalam, P. C.; Gosvami, N. N.; Caporizzo, M. A.; Composto, R. J.; Carpick, R. W. Nano-Rheology of Hydrogels Using Direct Drive Force Modulation Atomic Force Microscopy. *Soft Matter* **2015**, *11*, 8165–8178.

(105) Alcaraz, J.; Buscemi, L.; Puig-de Morales, M.; Colchero, J.; Baró, A.; Navajas, D. Correction of Microrheological Measurements of Soft Samples with Atomic Force Microscopy for the Hydrodynamic Drag on the Cantilever. *Langmuir 18*, 716–721.

View Article Online
DOI: 10.1039/D5NR01790D

(106) Piacenti, A. Atomic Force Microscope-Based Methods for the Nano-Mechanical Characterisation of Hydrogels and other Viscoelastic Polymeric Materials for Biomedical Applications. 2021.

(107) Piacenti, A. R.; Adam, C.; Hawkins, N.; Wagner, R.; Seifert, J.; Taniguchi, Y.; Proksch, R.; Contera, S. Nanoscale Dynamic Mechanical Analysis over a Broad and Continuous Frequency Range using Photothermal Actuation Atomic Force Microscopy. *Macromolecules* **2024**, *57*, 1118–1127.

(108) Schäffer, T. E.; Cleveland, J. P.; Ohnesorge, F.; Walters, D. A.; Hansma, P. K. Studies of vibrating atomic force microscope cantilevers in liquid. *Journal of Applied Physics 80*, 3622–3627.

(109) Rabe, U.; Hirsekorn, S.; Reinstädtler, M.; Sulzbach, T.; Lehrer, C.; Arnold, W. Influence of the cantilever holder on the vibrations of AFM cantilevers. *Nanotechnology 18*, 044008.

(110) Labuda, A.; Cleveland, J.; Geisse, N. A.; Kocun, M.; Ohler, B.; Proksch, R.; Viani, M. B.; Walters, D. Photothermal Excitation for Improved Cantilever Drive Performance in Tapping Mode Atomic Force Microscopy. *Microsc. Anal.* **2014**, *28*, 21–25.

(111) Nalam, P. C.; Gosvami, N. N.; Caporizzo, M. A.; Compostob, R. J.; Carpick, R. W. Nano-Rheology of Hydrogels Using Direct Drive Force Modulation Atomic Force Microscopy. *Soft Matter* **2015**, *11*, 8165–8178.

(112) Folkman, J.; Moscona, A. Role of cell shape in growth control. *Nature 273*, 345–349.

(113) Montheard, J.-P.; Chatzopoulos, M.; Chappard, D. 2-Hydroxyethyl Methacrylate (HEMA): Chemical Properties and Applications in Biomedical Fields. *Journal of Macromolecular Science, Part C: Polymer Reviews 32*, 1–34.

View Article Online
DOI: 10.1039/D5NR01790D

(114) Serban, M. A.; Liu, Y.; Prestwich, G. D. Effects of extracellular matrix analogues on primary human fibroblast behavior. *Acta Biomaterialia 4*, 67–75.

(115) Yang, J.; Nandi, S. *International Review of Cytology*; Elsevier, Vol. 81; pp 249–286.

(116) Verzár, F. *International Review of Connective Tissue Research*; Elsevier, Vol. 2; pp 243–300.

(117) Gautieri, A.; Vesentini, S.; Redaelli, A.; Buehler, M. J. Hierarchical Structure and Nanomechanics of Collagen Microfibrils from the Atomistic Scale Up. *Nano Letters 11*, 757–766.

(118) Williams, B. R.; Gelman, R. A.; Poppke, D. C.; Piez, K. A. Collagen fibril formation. Optimal in vitro conditions and preliminary kinetic results. *The Journal of Biological Chemistry 253*, 6578–6585.

(119) Stamov, D. R.; Pompe, T. Structure and function of ECM-inspired composite collagen type I scaffolds. *Soft Matter 8*, 10200.

(120) Engelmayr, G. C.; Papworth, G. D.; Watkins, S. C.; Mayer, J. E.; Sacks, M. S. Guidance of engineered tissue collagen orientation by large-scale scaffold microstructures. *Journal of Biomechanics 39*, 1819–1831.

(121) Zaman, M. H.; Trapani, L. M.; Sieminski, A. L.; Siemeski, A.; Mackellar, D.; Gong, H.; Kamm, R. D.; Wells, A.; Lauffenburger, D. A.; Matsudaira, P. Migration of tumor cells in 3D matrices is governed by matrix stiffness along with cell-matrix adhesion and proteolysis. *Proceedings of the National Academy of Sciences of the United States of America 103*, 10889–10894.

(122) Tian, Z.; Li, C.; Duan, L.; Li, G. Physicochemical properties of collagen solutions cross-linked by glutaraldehyde. *Connective Tissue Research 55*, 239–247.

View Article Online
DOI: 10.1039/D5NR01790D

(123) Franco-Barraza, J.; Beacham, D. A.; Amatangelo, M. D.; Cukierman, E. Preparation of Extracellular Matrices Produced by Cultured and Primary Fibroblasts. *Current Protocols in Cell Biology 71*.

(124) Ruijgrok, J. M.; De Wijn, J. R.; Boon, M. E. Optimizing glutaraldehyde crosslinking of collagen: effects of time, temperature and concentration as measured by shrinkage temperature. *Journal of Materials Science: Materials in Medicine 5*, 80–87.

(125) Olde Damink, L. H. H.; Dijkstra, P. J.; Van Luyn, M. J. A.; Van Wachem, P. B.; Nieuwenhuis, P.; Feijen, J. Glutaraldehyde as a crosslinking agent for collagen-based biomaterials. *Journal of Materials Science: Materials in Medicine 6*, 460–472.

(126) Chandran, P. L.; Paik, D. C.; Holmes, J. W. Structural Mechanism for Alteration of Collagen Gel Mechanics by Glutaraldehyde Crosslinking. *Connective Tissue Research 53*, 285–297.

(127) Karpushkin, E.; Dušková-Smrčková, M.; Remmler, T.; Lapčíková, M.; Dušek, K. Rheological properties of homogeneous and heterogeneous poly(2-hydroxyethyl methacrylate) hydrogels. *Polymer International 61*, 328–336.

(128) Baït, N.; Derail, C.; Benaboura, A.; Grassl, B. Rheology and adhesive properties versus structure of poly(acrylamide-co-hydroxyethyl methacrylate) hydrogels. *International Journal of Adhesion and Adhesives 96*, 102449.

(129) Janáček, J. Mechanical Behavior of Hydroxyalkyl Methacrylate Polymers and Copolymers. *Journal of Macromolecular Science, Part C: Polymer Reviews 9*, 3–47.

(130) Lewis, C. L.; Anthamatten, M. Synthesis, swelling behavior, and viscoelastic properties of functional poly(hydroxyethyl methacrylate) with ureidopyrimidinone side-groups. *Soft Matter 9*, 4058.

View Article Online
DOI: 10.1039/D5NR01790D

(131) Stevenson, W. T. K.; Sefton, M. V. The equilibrium water content of some thermoplastic hydroxyalkyl methacrylate polymers. *Journal of Applied Polymer Science 36*, 1541–1553.

(132) Salomé Machado, A. A.; Martins, V. C. A.; Plepis, A. M. G. Thermal and Rheological Behavior of Collagen. Chitosan blends. *Journal of Thermal Analysis and Calorimetry 67*, 491–498.

(133) Knapp, D. M.; Barocas, V. H.; Moon, A. G.; Yoo, K.; Petzold, L. R.; Tranquillo, R. T. Rheology of reconstituted type I collagen gel in confined compression. *Journal of Rheology 41*, 971–993.

(134) Brazdaru, L.; Micutz, M.; Staicu, T.; Albu, M.; Sulea, D.; Leca, M. Structural and rheological properties of collagen hydrogels containing tannic acid and chlorhexidine digluconate intended for topical applications. *Comptes Rendus Chimie 18*, 160–169.

(135) Zuidema, J. M.; Rivet, C. J.; Gilbert, R. J.; Morrison, F. A. A protocol for rheological characterization of hydrogels for tissue engineering strategies: A Protocol for Rheological Characterization of Hydrogels. *Journal of Biomedical Materials Research Part B: Applied Biomaterials 102*, 1063–1073.

(136) Roca-Cusachs, P.; Almendros, I.; Sunyer, R.; Gavara, N.; FarrÃĺ, R.; Navajas, D. Rheology of Passive and Adhesion-Activated Neutrophils Probed by Atomic Force Microscopy. *Biophysical Journal 91*, 3508–3518.

(137) PureCol EZ Gel solution. `https://www.sigmaaldrich.com/catalog/product/sigma/5074?lang=en&region=GB`, Sigma-Aldrich Preparation Note. https://www.sigmaa ldrich.com/catalog/product/sigma/5074?lang=en&region=GB.

(138) Corporation, L. T. Live Cell Imaging Solution Quick Start Guide. Molecular Probes: Eugene, OR< USA, 2011.

View Article Online
DOI: 10.1039/D5NR01790D

(139) Fernandez Davila, J. G.; Singh, A. K.; Moore, D. W. .; Kim, J.; Khan, J. A.; Lemma, M.; King, C. S.; Nathan, S. D.; Rodriguez, L. R.; Grant, G. M.; Moran, J. L. Pulmonary matrix-derived hydrogels from patients with idiopathic pulmonary fibrosis induce a proinflammatory state in lung fibroblasts in vitro. *Molecular Biology of the Cell 35*, ar114.

(140) Tian, Z.; Liu, W.; Li, G. The microstructure and stability of collagen hydrogel cross-linked by glutaraldehyde. *Polymer Degradation and Stability 130*, 264–270.

(141) Nashchekina, Y. A.; Lukonina, O. A.; Darvish, D. M.; Nashchekin, A. V.; Elokhovskii, V. Y.; Yudin, V. E.; Mikhailova, N. A. Biological and Rheological Properties of Collagen Cross-Linked with Glutaraldehyde. *Technical Physics* **2020**, *65*, 1535–1540.

(142) Constable, M.; Burton, H.; Lawless, B.; Gramigna, V.; Buchan, K.; Espino, D. Effect of glutaraldehyde based cross-linking on the viscoelasticity of mitral valve basal chordae tendineae. *BioMedical Engineering OnLine* **2018**, *17*.

(143) Applications Guide Version 16 Revision. Oxford Instruments Asylum Research Manual.

(144) Lakes, R. S. Viscoelastic measurement techniques. *Review of Scientific Instruments* **2004**, *75*, 797–810.

(145) Hertz, H. Ueber die Berührung fester elastischer Körper. *Journal für die reine und angewandte Mathematik (Crelles Journal) 1882*, 156–171.

(146) Adam, C. Physical Regulation of Cell Behaviors: Multifrequency AFM Measurement of Mechanoelectric, Mechanochemical, and Hydration Shell Effects on ECM and Cell Substrate Viscoelasticity. 2021.

View Article Online
DOI: 10.1039/D5NR01790D

(147) Higgins, M. J.; Proksch, R.; Sader, J. E.; Polcik, M.; Mc Endoo, S.; Cleveland, J. P.; Jarvis, S. P. Noninvasive determination of optical lever sensitivity in atomic force microscopy. *Review of Scientific Instruments* **2006**, *77*, 013701.

(148) Get Real - Automated Probe Calibration. Oxford Instruments Asylum Research Forums. https://support.asylumresearch.com/articles/video-tutorials-aa/19721-getreal-automated-probe-calibration. 2014.

(149) Chen, W.-L.; Cordero, R.; Tran, H.; Ober, C. K. *50th Anniversary Perspective* : Polymer Brushes: Novel Surfaces for Future Materials. *Macromolecules 50*, 4089–4113.

(150) Dokukin, M. E.; Kuroki, H.; Minko, S.; Sokolov, I. AFM Study of Polymer Brush Grafted to Deformable Surfaces: Quantitative Properties of the Brush and Substrate Mechanics. *Macromolecules 50*, 275–282.

(151) Jalili, K.; Abbasi, F.; Behboodpour, L. In situ probing of switchable nanomechanical properties of responsive high-density polymer brushes on poly(dimethylsiloxane): An AFM nanoindentation approach. *Journal of the Mechanical Behavior of Biomedical Materials 93*, 118–129.

(152) Üzüm, C.; Hellwig, J.; Madaboosi, N.; Volodkin, D.; von Klitzing, R. Growth behaviour and mechanical properties of PLL/HA multilayer films studied by AFM. *Beilstein Journal of Nanotechnology 3*, 778–788.

(153) Gutsmann, T.; Hassenkam, T.; Cutroni, J. A.; Hansma, P. K. Sacrificial Bonds in Polymer Brushes from Rat Tail Tendon Functioning as Nanoscale Velcro. *Biophysical Journal 89*, 536–542.

(154) Contera, S. A.; Voïtchovsky, K.; Ryan, J. F. Controlled ionic condensation at the surface of a native extremophile membrane. *Nanoscale 2*, 222–229.

View Article Online
DOI: 10.1039/D5NR01790D

(155) Voïtchovsky, K.; Kuna, J. J.; Contera, S. A.; Tosatti, E.; Stellacci, F. Direct mapping of the solid-liquid adhesion energy with subnanometre resolution. *Nature Nanotechnology 5*, 401–405.

(156) Gavara, N.; Chadwick, R. S. Determination of the elastic moduli of thin samples and adherent cells using conical atomic force microscope tips. *Nature Nanotechnology 7*, 733–736.

(157) Roylance, D. Engineering Viscoelasticity. Massachusetts Institute of Technology. https://web.mit.edu/course/3/3.11/www/modules/visco.pdf.

(158) Menard, K. *Dynamic Mechanical Analysis: A Practical Introduction*, 2nd ed.; CRC Press, 2008.

(159) Zhang, Y. Z.; Adam, C.; Rehnstrom, H.; Contera, S. Temporal evolution of mechanical properties in PDMS: A comparative study of elastic modulus and relaxation time for storage in air and aqueous environment. *Journal of the Mechanical Behavior of Biomedical Materials* **2024**, *160*, 106779.

(160) Akhtar, R.; Sherratt, M. J.; Cruickshank, J. K.; Derby, B. Characterizing the elastic properties of tissues. *Materials Today 14*, 96–105.

(161) Beni, E. A.; Shahidi, A.; Ebadian, B. Mechanical properties of mandibular and maxillary bone collagen fibrils based on nonlocal elasticity theory. *Biophysical Reports 5*, 100210.

(162) Garcia-Sacristana, C.; Garcia, R. Time-lapsed nanoscale maps of the elastic modulus of collagen during cross-linking by bimodal AFM. *Nanoscale*

(163) Dutov, P.; Antipova, O.; Varma, S.; Orgel, J. P. R. O.; Schieber, J. D. Measurement of Elastic Modulus of Collagen Type I Single Fiber. *PLOS ONE 11*, e0145711.

View Article Online
DOI: 10.1039/D5NR01790D

(164) Yang, L.; van der Werf, K. O.; FitiÃľ, C. F.; Bennink, M. L.; Dijkstra, P. J.; Feijen, J. Mechanical Properties of Native and Cross-linked Type I Collagen Fibrils. *Biophysical Journal 94*, 2204–2211.

(165) Athenstaedt, H. Permanent electric polarization of the meninges of man. *Zeitschrift für Zellforschung und Mikroskopische Anatomie 98*, 300–322.

(166) Athenstaedt, H. Pyroelectric and Piezoelectric Properties of Vertebrates. *Annals of the New York Academy of Sciences 238*, 68–94.

(167) Athenstaedt, H. Permanent electric polarization and pyroelectric behaviour of the vertebrate skeleton: III. The axial skeleton of man. *Zeitschrift fi£¡r Zellforschung und Mikroskopische Anatomie 93*, 484–504.

(168) Ferry, J. D. *Viscoelastic properties of polymers*, 3rd ed.; Wiley, 1980.

(169) Seifert, J.; Kirchhelle, C.; Moore, I.; Contera, S. Mapping cellular nanoscale viscoelasticity and relaxation times relevant to growth of living Arabidopsis thaliana plants using multifrequency AFM. *Acta Biomaterialia* **2021**, *121*, 371–382.

(170) Labernadie, A.; Bouissou, A.; Delobelle, P.; Balor, S.; Voituriez, R.; Proag, A.; Fourquaux, I.; Thibault, C.; Vieu, C.; Poincloux, R.; CharriÃÍre, G. M.; Maridonneau-Parini, I. Protrusion force microscopy reveals oscillatory force generation and mechanosensing activity of human macrophage podosomes. *Nature Communications 5*, 5343.

(171) Chen, D.-C.; Lai, Y.-L.; Lee, S.-Y.; Hung, S.-L.; Chen, H.-L. Osteoblastic response to collagen scaffolds varied in freezing temperature and glutaraldehyde crosslinking. *Journal of Biomedical Materials Research Part A 80A*, 399–409.

(172) Haugh, M. G.; Murphy, C. M.; McKiernan, R. C.; Altenbuchner, C.; O'Brien, F. J. Crosslinking and Mechanical Properties Significantly Influence Cell Attachment, Pro-

View Article Online
DOI: 10.1039/D5NR01790D

liferation, and Migration Within Collagen Glycosaminoglycan Scaffolds. *Tissue Engineering Part A 17*, 1201–1208.

(173) Brooks, P. J.; Glogauer, M.; McCulloch, C. A. An Overview of the Derivation and Function of Multinucleated Giant Cells and Their Role in Pathologic Processes. *The American Journal of Pathology 189*, 1145–1158.

(174) Chambers, T. J. Multinucleate giant cells. *The Journal of Pathology 126*, 125–148.

View Article Online
DOI: 10.1039/D5NR01790D

Data availability

The datasets supporting the findings of this study are not publicly available at the time of publication but can be obtained from the corresponding author upon reasonable request.